Accepted Manuscript

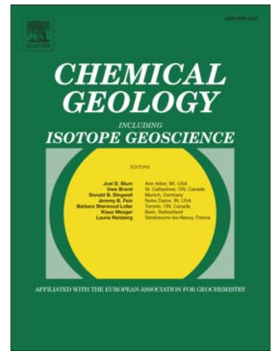

Evidence for channelized external fluid flow and element transfer in subducting slabs (Raspas Complex, Ecuador)

Petra Herms, Timm John, Ronald J. Bakker, Volker Schenk

PII:	S0009-2541(12)00148-9
DOI:	doi: 10.1016/j.chemgeo.2012.03.023
Reference:	CHEMGE 16489
To appear in:	*Chemical Geology*
Received date:	9 February 2011
Revised date:	29 February 2012
Accepted date:	26 March 2012

Please cite this article as: Herms, Petra, John, Timm, Bakker, Ronald J., Schenk, Volker, Evidence for channelized external fluid flow and element transfer in subducting slabs (Raspas Complex, Ecuador), *Chemical Geology* (2012), doi: 10.1016/j.chemgeo.2012.03.023

Evidence for channelized external fluid flow and element transfer in subducting slabs (Raspas Complex, Ecuador)

Herms, Petra[1,*], John, Timm[1,2], Bakker, Ronald J[3], Schenk, Volker[1]

1. Institut für Geowissenschaften and SFB 574, Universität Kiel, Olshausenstr. 40, 24098 Kiel, Germany; (ph@min.uni-kiel.de), (vs@min.uni-kiel.de)
2. Institut für Mineralogie, Universität Münster, Corrensstr. 24, 48149 Münster, Germany; (timm.john@uni-muenster.de)
3. Department Applied Geosciences & Geophysics, Mineralogy & Petrology, University of Leoben, Peter-Tunner-Str.5, 8700 Leoben, Austria; (Ronald.Bakker@mu-leoben.at)

Abstract

Fluids released at great depth by dehydrating subducting plates play a major role in mass transport and are responsible for metasomatism and partial melting in the overlying mantle wedge. To investigate the fluid-flow regime and element mobility within a subducting oceanic lithosphere, the Raspas Complex in Ecuador has been selected where an ophiolite association of blueschists, eclogites, metapelites and ultramafitites is exposed. This ophiolite association stands out by high-pressure zoisite veins, associated metasomatized zoisite eclogites and deserpentinized, pseudo-spinifex textured chlorite harzburgites indicating fluid flow and element mobility at depth of about 60 km. Oscillatory zoning in vein zoisite and garnet rims in the metasomatized eclogites is explained by cyclic fluid expulsion during high-pressure deserpentinization after overstepping of the antigorite breakdown reaction. Fluid inclusion studies reveal a homogeneous low-salinity aqueous fluid composition with minor CH_4 and CO_2 which is in accord with open-system fluid infiltration derived from an external source. The deserpentinized chlorite harzburgite is a potential source for the low-salinity aqueous fluid. The association of zoisite veins with zoisite eclogites which are enriched in LREE, MREE, Pb, Sr, HFSE, Th, U, compared to MORB-type eclogites, documents the metasomatic effects and the fluid mobility of a large range of trace elements. In addition, the fluid-mobile trace elements B, Rb, Pb, Sr are enriched in fluid inclusions in omphacite. Most trace elements cannot be derived from the serpentinites but might be explained by leaching from metabasites and metapelites in zones of intense fluid-rock interaction. A garnet-amphibole rock, deficient in LREE, MREE and Sr, could represent such a leached metabasite.

B, Rb, Th and U could be derived from metapelites. By channelized fluid flow and high fluid flux, the fluid-mobile trace elements might be transported into the mantle wedge.

1. Introduction

In subduction zones, oceanic lithosphere descends to great depth while being modified by metamorphic reactions. Devolatilization reactions due to increasing temperatures lead to the liberation of aqueous fluids (Schmidt and Poli, 1998). These fluids may enter the mantle wedge inducing partial melting and, ultimately, volcanism at convergent plate margins. The typical geochemical signature of arc magmas above subduction zones indicates a contribution of slab components, implying some degree of element transport from the slab to the mantle wedge (Plank and Langmuir, 1993; Elliott, 2003). The main source of fluids at sub-arc depth could be serpentinized lithosphere (Rüpke et al., 2002; Schmidt and Poli, 2003). However, direct evidence for ultimate dehydration of serpentinitic rocks in the subduction zone has only been reported from the Almirez Massif, Spain (Trommsdorff et al., 1998; Puga et al., 1999; Lopez Sanchez-Vizcaino et al., 2005).

Essential insights into the nature and composition of fluids at great depths in subduction zones is offered by the direct observation of synmetamorphic fluid remnants preserved as primary fluid inclusions in high-pressure rocks. In an extensive review of fluid inclusion studies in eclogite-facies rocks, Klemd (2004) showed that aqueous fluids with varying salinities dominate, whereas CO_2-rich or CH_4-N_2-rich aqueous fluid inclusions are less abundant (Selverstone et al., 1992; Herms, 2002; Fu et al., 2003; Shi et al., 2005). However, combined evidence from experiments and natural rocks indicates that the original high-pressure fluids liberated by dehydration are aqueous with low salinities, whereas a high variability in fluid inclusion composition is rather due to intense fluid-rock interaction and modifications during retrograde metamorphism and exhumation (Scambelluri et al., 1997; Gao and Klemd, 2001; Hermann et al., 2006).

Information on the trace-element content of high-pressure fluids can come from appropriate fluid inclusions, experimentally determined distribution coefficients, or the study of metasomatic changes at the contact of high-pressure rocks with transport veins. There are few studies that report the trace-element composition of fluid inclusions in eclogite-facies rocks, veins and subducted serpentinites (e.g., Scambelluri et al., 2001; Hermann et al., 2006). These studies show that the fluid is enriched in LILE, Pb, Sr, Th and U. Recent experimental studies by Spandler et al. (2007) using synthetic fluid/melt inclusions show that the hydrous fluids at 600 and 650°C and 2.2 GPa have relatively high LILE contents compared to REE and HFSE although all elements preferentially partition into the metapelite residue. Based on these results, they conclude that slab dehydration fluids are probably too dilute to account for the trace-element budget of arc magmas. Spandler et al. (2004) and Hermann et al. (2006) came to similar conclusions based on trace-element studies on bulk rock samples of subducted mafic rocks. Specifically, aqueous fluids released by dehydration during the blueschist to eclogite transition contain only moderate amounts of LILE, Sr, and Pb and do not significantly mobilize LREE, U and Th. This suggests that at low fluid flux the overall mass transfer is low (Zack and John, 2007).

Evidence for element mobility at great depths includes high-pressure veins in eclogite-facies rocks, and their composition may reveal important information about the processes of element transport between slab and mantle. In fact, long-distance transport veins due to channelized fluid flow and high fluid flux are able to transport a large amount of trace elements, even those considered as relatively immobile (REE, HFSE, U, Th) (Bebout and Barton, 1993; Gao et al., 2007; John et al., 2004, 2008; Beinlich et al., 2010). In zones of intense fluid-rock interaction, external fluids derived from deserpentinization of underlying mantle lithosphere can dissolve large quantities of trace elements from the oceanic crust and sediment during transport to the mantle wedge (Bebout and Barton, 1993; John et al., 2004, 2008).

With this study, we attempt to characterize fluid and element transport as well as metasomatic effects in subducted lithosphere. High-pressure zoisite veins intersecting and infiltrating eclogites of the Raspas Complex, Ecuador, provide an opportunity to study fluid mobility within the slab at a depth of 60-70 km. Newly discovered chlorite harzburgites with pseudo-spinifex texture provide strong evidence for deserpentinization, similar to the Almirez Complex (Trommsdorff et al. 1998), and thus are a probable fluid source. We present new petrology, bulk rock and mineral geochemistry, and fluid inclusion data. Accompanying Sr-, Nd-, Li-, O-, and N-isotope studies demonstrate the metasomatic effects (Halama et al., 2010, 2011). Here, we will show that the zoisite veins served as channelways for external aqueous fluids, which infiltrated and metasomatized the wall-rock eclogites. We will discuss the different possible sources of the fluid and their trace elements.

2. Geology and field relationships

The Raspas Complex, situated in the southwestern part of Ecuador (Fig. 1), is a rare occurrence of high-pressure rocks in the Andes (e.g., Feininger, 1980, 1982). It consists of ultramafic rocks of the El Toro Formation and of eclogites, blueschists and intercalated metapelites of the Raspas Formation. The ultramafic rocks of the El Toro Formation are interpreted to present depleted MORB-source mantle (John et al., 2010). They underwent similar metamorphic conditions as the eclogites of the El Toro Formation (Gabriele et al., 2002). The metapelites of the Raspas Formation are graphite-bearing schists containing the high-pressure assemblage garnet+chloritoid+kyanite+phengite+quartz (Gabriele et al., 2003), and are thought to represent mainly subducted forearc sediments (Bosch et al., 2002). The protoliths of the eclogites in the Raspas Formation are tholeiitic MOR basalts whereas the blueschists have seamount-like element signatures. Both rock types are cofacial and experienced the same peak *P*-*T* conditions, but different mineral assemblages developed due to distinctly higher Al and lower Fe contents in the blueschists (John et al., 2010).

The Raspas Complex represents oceanic lithosphere sandwiched between the continental Biron Terrane to the North and the oceanic Arenillas-Panupali Unit to the South (Feininger, 1978, 1987; Gabriele, 2002). The Raspas Complex can be regarded as a fragment of a paleosubduction zone (Aspden et al. (1995), active from the latest Jurassic to Early Cretaceous. Phengite K–Ar data (Feininger, 1980) and Ar–Ar data (Gabriele, 2002) gave cooling ages of 132±5 Ma and 123–129 Ma, respectively, for the high-pressure metamorphic event. Lu–Hf dating of high-pressure garnet growth by John et al. (2010) gave similar ages at around 130 Ma for blueschist, metapelite and eclogite. According to geothermobarometry (Gabriele, 2002; Gabriele et al., 2002, 2003; John et al., 2010; Smye et al., 2010), eclogites and metapelites of the Raspas Complex reached peak *P*–*T* conditions of about 1.5-2.3 GPa and 550-650°C, indicating a subduction depth of about 60-70 km. During uplift the rocks were locally subjected to greenschist-facies retrogression, but the eclogite-facies mineral assemblages and textures have generally been preserved. The close association of MORB-mantle-like peridotites, eclogitic MORB-type metabasites, metasedimentary rocks with oceanic affinity, and blueschists interpreted to have seamount protoliths defines the Raspas Complex as a deeply subducted ophiolite complex (John et al., 2010).

The outcrops are limited due to dense vegetation and those suitable for sampling are found only along the river Raspas, where an interrupted cross-section exposes eclogites in the north to ultramafic rocks in the south (Fig. 1). The eclogites show a well-developed schistosity, generally striking E-W and steeply dipping to the north (Gabriele, 2002). The rocks are tightly folded, often with isoclinal folds, with fold axes dipping to SW. Garnet-amphibole rocks occur locally and show gradual transitions to the eclogites. Few layers of metasediments up to 10 m wide are found intercalated in the eclogitic rock suite. At one locality near the boundary with the ultramafic rocks, a coherent section of eclogites is cut by several zoisite veins up to dm-wide and several meters long, pervasively intruding the outcrop without apparent start or end points (Fig. 2). The zoisite-bearing eclogites of this locality are referred to as “zoisite eclogites” hereafter. The approximately N-S striking zoisite veins are up to dm-wide and cut the schistosity of the eclogites discordantly (Fig. 2). The ultramafic rocks in the southern part of the cross-section show similar banding, schistosity (E-W striking, steeply dipping) and tight folding as the eclogites (Gabriele, 2002). Variably serpentinized peridotite layers alternate with amphibole-chlorite rich deserpentinized layers. A peculiar chlorite-tremolite harzburgite with pseudo-spinifex texture is exposed in a 150 m-wide outcrop near the zoisite eclogites. Longitudes and latitudes of the sample locations are given in Appendix C. Because of the poor outcrop situation, not only bedrock samples have been taken, but also some samples from boulders which have been transported downstream for some distance (Fig. 1).

3. Sample description

The petrography and mineral chemistry including photomicrographs and X-ray element maps are given in the Appendices A, B and C. The chemical formulae and abbreviations of minerals and mineral end-members used in this section are found in Appendix C. In the following, a short description of the studied rock samples is given.

3.1. MORB-type eclogites

The MORB-type eclogites are fine- to medium-grained, banded rocks with a distinct stretching lineation. Major mineral phases are garnet, omphacite and amphibole. Minor and accessory phases include rutile, quartz, phengite, carbonate and clinozoisite. Garnet blasts are distinctly zoned with Fe-, Mn- and Ca-rich cores whereas the rims are rich in Mg but poor in Fe, Mn and Ca. All minerals of the matrix occur as inclusions in garnet, however, omphacite is present only in the garnet rim. In additon, albite and titanite are enclosed in the garnet core. Omphacite with 36–44 mol% jadeite component is found in textural equilibrium with Mg-katophoritic to barroisitic amphibole. Geochemically, the MORB-type eclogites are basaltic (44–50 mass% SiO_2) with LREE-depleted (La_N/Yb_N = 0.49–0.72) chondrite-normalized REE patterns and trace-element signatures typical for N-MORB (John et al., 2010).

3.2. Zoisite eclogites and zoisite veins

The zoisite eclogites contain 5–20 vol.% coarse-grained zoisite in textural equilibrium with garnet, omphacite, minor amphibole, rutile and carbonate. The rocks are cut by numerous zoisite veins of mm- to dm-thickness (Fig. 2). In the vicinity of the veins, the zoisite eclogites are heterogeneously deformed whereby the primary banding and schistosity is largely obscured. In terms of major element composition, the zoisite eclogites are basaltic (45.2–48.5 mass% SiO_2) with high CaO (13.0–13.7 mass%) and Al_2O_3 (14.7–16.9 mass%), and low MgO (5.1–6.2 mass%) compared to the MORB-type eclogites (Halama et al, 2010). The zoisite veins are mostly monomineralic (>90 vol% zoisite), consisting of coarse, randomly oriented zoisite grains. In some parts of broader veins, euhedral zoisite crystals and interstitial albite indicate growth in an open space. The zoisite veins themselves are slightly deformed. The whole-rock vein composition is characterized by low SiO_2 (43.8 mass%), MgO (0.2 mass%), Na_2O (1.5 mass%) and K_2O contents (1.2 mass%), whereas Al_2O_3 (28.4 mass%) and CaO (19.8 mass%) are high (Halama et al, 2010). Albite veinlets associated with Mg-hornblende are observed locally in ruptured areas of the zoisite eclogite and in the zoisite veins. In addition, some late veinlets contain albite, K-feldspar, chlorite, actinolite, epidote and calcite.

Zoisite in the eclogite and in the veins appears inhomogeneous in composition due to a complex sector and oscillatory zoning pattern (Fig. 3). The Fe and Sr contents of zoisite in the vein and in the eclogite matrix are in a similar range (1.1–3.6 mass% Fe_2O_3, 0.3–0.8 mass% SrO). Additional trace-element data are reported in Section 6.

Garnet grains in the zoisite eclogite show an overall decrease in Fe and Mn from core to rim typical for prograde zoning. With respect to Ca, zoning in the core is similar as in garnet grains of the MORB-type eclogites. However, garnet porphyroblasts in the zoisite eclogites are characterized by an outer rim (Rim 2) with oscillatory zoning and overall increasing Ca up to 35 mol% Grs which appears to have overgrown the Ca-poor garnet rim of the MORB-type eclogites (Fig. 4A). Where garnet grains are cut by a zoisite vein, the grossular-rich Rim 2 is found at the contact with the vein (Fig. 4C-E). Specific mineral inclusions are correlated with garnet zoning: (A) albite, calcite, quartz and graphite inclusions in the core, (B) omphacite beside albite and very small ankerite inclusions in Rim 1, (C) omphacite, zoisite/clinozoisite and hornblende inclusions in Rim 2.

Omphacite in the zoisite eclogite shows fine-scale patchy compositional inhomogeneities, generally in the range 31–45 mol% Jd (Fig. 4B). In deformed and polygonized domains, the omphacite composition is more homogeneous and jadeite-rich (40–48 mol% Jd). Omphacite in contact with albite veinlets is still high in jadeite content (~40 mol% Jd) except in a few places where μm-thin diopside-rich rims developed.

3.3. Garnet-amphibole rocks

Main constituents of these banded and schistose rocks are garnet and amphibole whereas omphacite (35 mol% Jd) is only found as corroded relics. Accessory phases are rutile and quartz. Garnet shows limited compositional variability ($Alm_{48–57}Prp_{19–24}Sps_1Grs_{22–28}$), amphibole is magnesiohornblende or barroisite. The garnet-amphibole rocks are high in Fe_2O_3 but low in CaO, Na_2O and SiO_2 contents compared to the MORB-type eclogites (John et al., 2010).

3.4. Ultramafitites

Three ultramafic rock types are distinguished on the basis of mineralogy and texture: (1) The most common antigorite-chlorite peridotites contain porphyroclasts of olivine (X_{Mg} = 0.88-0.89) intergrown with Ti-clinohumite, orthopyroxene and clinopyroxene (Cr-diopside) in a schistose matrix of antigorite, chlorite and magnetite. The degree of serpentinization varies from almost pristine peridotites to serpentinites with about 90 vol.% antigorite. Cr-diopside porphyroclasts are marginally recrystallized to Cr-poor diopside. (2) Tremolite-chlorite peridotites contain porphyroclasts of olivine and orthopyroxene, whereas primary clinopyroxene is largely replaced by neoblastic diopside and tremolite. In the fine-grained matrix, recrystallized olivine (X_{Mg} = 0.87) is in contact with tremolite and Cr-bearing chlorite. (3) One peculiar sample of chlorite harzburgite (SEC 41-2) shows large fan-shaped aggregates of orthopyroxene rods (Fig. 5) and cm-sized elongated olivine grains, both set in a matrix of mm-sized chlorite and minor tremolite. This texture strongly resembles the pseudo-spinifex texture of chlorite harzburgites from the Almirez Massif described by Trommsdorff et al. (1998). Locally, clusters of carbonate (dolomite and magnesite) occur. In contrast to orthopyroxene porphyroclasts, orthopyroxene of the fan-shaped aggregates is very poor in Ca, Al and Cr. Olivine (X_{Mg} = 0.87) is partially serpentinized along late veins containing talc, chrysotile and magnetite.

4. Analytical methods

In-situ trace-element analyses of minerals were conducted by LA-ICP-MS at the University of Würzburg using a Merchantek 266 LUV (266 nm) laser and a quadrupole Agilent 7500c ICP-mass spectrometer. Spot analyses were applied with a laser repetition rate of 10 Hz and an energy of 0.36-0.54 mJ. Spot sizes were 40 µm. The regular setting of the laser source, mass spectrometer and standardizing procedures have been described in detail by Schulz et al. (2006). The calculation of trace-element concentrations was conducted by the

GLITTER Version 3.0 online interactive data reduction for LA-ICP-MS Program (Macquarie Research Ltd, 2000). The 1-sigma error is based on counting statistics from signal and background with dependence on the absolute concentration. The glass reference material NIST SRM 612 was used for external calibration using values of Pearce et al. (1997). For the silicate minerals, ^{29}Si was used as internal standard taking the SiO_2 concentration as determined by microprobe analyses. Accuracy and precision of the method were determined by repeated analysis of the NIST SRM 610 and 614 standards measured as unknown samples. Precision was usually better than 10 % for all elements. Although the accuracy of the mineral analyses could be less due to matrix effects (e.g., Kroslakova and Günther, 2007), the main results concerning the variability of trace elements within specific minerals due to zonation will not be affected.

Microthermometric measurements of fluid inclusions were carried out with a Linkam THM 600 heating/freezing stage on 120–150 µm-thick double-polished wafers. Temperature was calibrated using a set of synthetic inclusions, distributed by Fluid Inc., USA, in the temperature interval from -56.6°C to 0.0°C. The temperature measurements are reproducible within ±0.2°C in the range -60 to +100°C, within ±0.5-2°C in the range -60 to -120°C, within ±3°C in the range -120 to -140°C and within about ±2°C above +100°C.

Raman microanalyses were made with a Dilor LABRAM confocal Raman spectrometer at the University of Leoben, Austria, equipped with a frequency-doubled Nd-YAG laser (100 mW, 532.2 nm) and with an LMPlanFI 100x/0.80 objective lens (Olympus). The laser beam was focussed on the bubble, the surrounding liquid and, if present, on included crystals. The volume of the focus-spot of the laser has a diameter of ±6 µm, using a 100 times objective. Depending on the host mineral, the counting time varied in the range 10-60 s, except for small hydrocarbon-bearing inclusions in clinopyroxene (600 s). The wavenumbers are calibrated with the Raleigh scattering (0 cm^{-1}), silicon (520.7 cm^{-1}), and polyethylene (main peaks at 1062.1, 1128.09, 1294.8, 1438.8, 2847.8, and 2880.9 cm^{-1}), by defining corrected wavenumbers in a linear best-fit equation of measured wavenumbers. Wavenumber measurements have an accuracy of 1.62 cm^{-1} at low $\Delta\nu$ (Raman shift around 0 cm^{-1}) and 1.1 cm^{-1} at high $\Delta\nu$ (around 3000 cm^{-1}).

To calculate the mole fractions, the molar volume, and the isochores of the H_2O–NaCl–CH_4 fluid inclusions, it was necessary to determine the ice- and clathrate-melting temperatures. Since ice and clathrate melting could not be distinguished by optical means, Raman spectrometry was applied during step-wise heating on a Linkam THMSG 600 stage. The spectra document the melting temperature of ice or clathrate by the disappearance of their peak. Based on the volume of the gas phase and the melting temperature of ice and clathrate, the composition of H_2O-rich fluid inclusions can be calculated in terms of X_{CH4}, X_{H2O} and salinity, using the program ICE from the software package CLATHRATES by Bakker (1997). However, for most fluid inclusions in the system H_2O–NaCl–CH_4, salinities were calculated from ice melting temperatures and the molar volumes from homogenization temperatures with the program BULK from the software package FLUIDS (Bakker, 2003) as being equivalent to a methane-free aqueous fluid. Molar volumes of pure methane fluid inclusions were calculated with the same program for the average homogenization temperature of -93.3°C. Isochore calculations based on molar volume and bulk fluid composition were obtained using the program ISOC from the software package FLUIDS (Bakker, 2003).

5. Fluid inclusion studies

5.1 Petrography

The zoisite veins, representing the fluid pathways of infiltrating fluids, as well as the associated zoisite-bearing eclogites offer the best opportunity to characterize the nature and composition of the subduction-related fluids. These rocks and veins contain abundant fluid inclusions in omphacite, zoisite and garnet. The MORB-type eclogites, in contrast, are mostly devoid of fluid inclusions.

In omphacite grains of the zoisite eclogites, the fluid inclusions are trapped in clusters in the core of the crystals (Fig. 6). They neither cut grain boundaries nor are they found on secondary fractures. The fluid inclusions occur in those parts of the omphacite which show the patchy compositional inhomogeneities. The strongly deformed and polygonized omphacite domains are free of fluid inclusions. Furthermore, no fluid inclusions are found near the contact to the albite veinlets, where diopside-rich rims develop. Mostly elongated in shape (5-10 µm in width, 10-40 µm in length), the fluid inclusions are oriented parallel to the c axis and thus parallel to the cleavage planes of the omphacite (Fig. 7A). In garnet, subhedral fluid inclusions occur in small groups or isolated in the rim zone (Fig. 7B) where also zoisite, omphacite and rutile inclusions are found. In zoisite of the eclogites and in vein zoisite, fluid inclusions often are dispersed all over the crystal (Fig. 7C) with variable shapes from elongated to tiny rounded or facetted to irregular shapes. Decrepitation features can also be found. In zoisite as well as in garnet, the average size of the fluid inclusions varies between 5 and 15 µm, whereas larger sizes up to 40 µm are exceptional. The fluid inclusions in omphacite, garnet and zoisite are two- to three-phase inclusions with a liquid, a gas bubble and commonly one or two mostly birefringent solids which constitute between about 5 and 30% of the fluid inclusion volume (Fig. 7A,B,D). The volume fraction of the vapour phase of the fluid inclusions is relatively constant with φ_{vap} about 0.1–0.2. Rarely in thin zoisite veins and in omphacite next to the veins, single-phase fluid inclusions occur (Fig. 7C). These inclusions are smaller in size (about 2–10 µm) and lie within the cluster of the two-phase fluid inclusions.

In the antigorite-chlorite peridotite, fluid inclusions are found in recrystallized clinopyroxene grains occurring as aggregates in an antigorite matrix. Very small fluid inclusions with sizes <5 µm are found in small clusters or occur in isolation (Fig. 7E). The shape is oval to round, sometimes with a visible bubble. In this case, the volume fraction φ_{vap} is about 0.1.

5.2 Microthermometry

Microthermometric analyses yield an aqueous composition of the two- and three-phase fluid inclusions in all minerals and rock types (see Appendix C). Most of the aqueous inclusions display freezing of the liquid phase below -40°C during cooling, accompanied by a sudden shrinkage of the vapour bubble. The initial, eutectic melting temperature upon heating (T_e) lies in the range -20 to -22°C indicating that NaCl is the main salt component of the aqueous inclusions. In all different host minerals of zoisite eclogite and zoisite vein samples, the fluid inclusions have relatively high final ice melting temperatures (T_m) indicating low salinities mainly in the range 0.4–5.3 eq mass% NaCl. This salinity estimation is based on a binary H_2O-NaCl system. The peak T_m(ice) value in the histogram shown in Fig. 8A lies at -1°C resulting in a mean salinity of about 2 eq mass% NaCl equivalents. Temperatures of clathrate melting in the range of +1 to +13 ˚C were determined in fluid inclusions in all minerals indicating the presence gases such as methane. Because of a refractive index very near to that of water, the colourless and isotropic clathrate crystals can hardly be optically detected except in large fluid inclusions. For a reliable identification of small clathrate crystals and for determination of the temperatures of phase transitions, Raman spectroscopy has been combined with low-temperature microthermometry (see Section 5.3). The bulk composition and density of individual fluid inclusions can be calculated from a combination of accurately determined T_m(ice), T_m(clathrate) and a volume fraction estimation of the vapour bubble at room temperatures (Bakker, 1997). As most aqueous fluid inclusions decrepitate or leak before homogenization into the liquid phase, homogenization temperatures were determined exemplarily on two samples. The few analyzed fluid inclusions display a variation in T_h (homogenization into the liquid phase) between 168 and 223°C in vein zoisite (Fig. 8B). An increase of the vapour-bubble size after homogenization and subsequent cooling to room temperature suggests that partial decrepitation after heating of these fluid inclusions occurred. A second type of fluid inclusion is one-phase at room temperature. These rare inclusions are gas-rich, and show homogenization temperatures from -87.3 to -98.0°C, which is typically for CH_4-rich gas mixtures. Microthermometric data for the fluid inclusions in serpentinized peridotite have not been obtained due to their extremely small size.

5.3 Raman spectrometry

Raman microspectrometric analyses were carried out on 34 fluid inclusions selected from aqueous low-salinity fluid inclusions in omphacite, zoisite and garnet. The presence of methane could be confirmed in all aqueous fluid inclusions in different eclogite-facies minerals in zoisite eclogites and veins. Representative spectra of these H_2O–NaCl–CH_4 fluid inclusions in different host minerals are shown in Fig. 9A-D. Exemplarily, one inclusion in vein zoisite has been analyzed by Raman spectrometry during heating and freezing of the sample (see Section 4). Applying this method, clathrate melting at +2.5°C, ice melting at -5°C, and a volume fraction of 0.2 for the vapour bubble after clathrate melting were determined. From these data, molar proportions of X_{H_2O} = 0.973, X_{CH_4} = 0.010, X_{NaCl} = 0.017 were obtained, corresponding to a salinity of 5.33 eq mass% NaCl (calculation method see Bakker, 1997). In the aqueous CH_4-bearing inclusions, most of the commonly observed birefringent solid phases were identified by Raman spectroscopy as calcite. Rarely, analcite was analyzed in fluid inclusions in omphacite, and mica in fluid inclusions in garnet. Extremely fine-grained opaque material common in the garnet cores was identified as graphite by Raman spectrometry. In addition to the ubiquitous water-rich inclusions, the small one-phase fluid inclusions in zoisite proved to be water-free CH_4 inclusions (Fig. 9B). Besides CH_4 minor ethane and tiny graphite flakes were identified.

We also tried to analyze fluid inclusions in clear diopside neoblasts in antigorite-chlorite peridotite in order to compare the fluid composition in eclogites and peridotites. However, most of these fluid inclusions are extremely small (<2 µm). Preliminary Raman spectrometric analyses were performed on a 3.5 µm sized fluid inclusion with a vapour bubble size of 1 µm. The Raman spectrum (Fig. 9D) shows peaks at wavenumbers of 2917, 2910 and 2941 cm^{-1} indicating that methane and hydrocarbon are present. A water peak is not obvious, due to a broad fluorescent shoulder at wavenumbers above 3000 cm^{-1} obscuring the Raman bands of H_2O.

5.4 Fluid isochores

Low-salinity aqueous fluid inclusions in different host minerals and samples yield a similar range of melting temperatures. As an example, isochores are calculated for inclusions in vein zoisite (Fig. 10). Several isochores were calculated in the pseudo-binary system H_2O-NaCl because clathrate melting temperatures were not detected in some inclusions, and because the previously described composition calculation results in a very low CH_4 content (<1 mol%). Assuming a similar CH_4-content for all aqueous fluid inclusions, the corresponding isochores would shift to lower pressures (approximately 150 MPa) at the same temperatures (Fig. 10). For pure CH_4 inclusions, the minor spread in isochores according to the variation in bulk densities (Fig. 10) illustrates relatively well-defined trapping conditions at low pressures.

6. Trace elements of zoisite and omphacite

The trace-element composition of zoisite in eclogites and veins, of omphacite in MORB-type and zoisite eclogite, and of fluid-inclusion-rich domains in omphacite were analysed by LA-ICP-MS (Table 1). The trace-element concentrations relative to chondrite and primitive mantle compositions, respectively, are displayed in REE spectra and spider diagrams (Fig. 11A, 12A).

The REE patterns of **zoisite** display a moderate decrease from very high LREE to still high MREE (up to Gd) and a strong decrease to HREE (Fig. 11A). There is a wide variation of LREE concentrations in the vein zoisite whereas in zoisite from the eclogite matrix the LREE concentrations are near the lower end of the values for vein zoisite. The Sr contents (2,700–8,200 µg/g) are similar to those determined by electron microprobe (see Section 4.2). Furthermore, high but variable concentrations of Pb (61–170 µg/g), Th (2–215 µg/g) and U (4–49 µg/g) were analysed (Fig. 12A). Since element mapping by microprobe has shown sector and oscillatory zoning in Sr and Fe content (Fig. 3A-C), similar zonation can also be assumed for Th, U and LREE, with even wider variations in concentrations as for Sr. This is indicated by largely different contents in those elements measured in different sectors within one zoisite grain (Table 1, SEC31-2-1, Analyses 20, 21). Because LA-ICP-MS analyses cover a relatively large part of the grain (about 40 µm), only bulk compositions in oscillatory-zoned grain domains are obtained. The HFSE, Li and Ba, occur in low concentrations and are obviously not incorporated in the zoisite structure (Fig. 12A).

The REE spectra for **omphacite** of the MORB-type eclogites show the typical bell-shaped pattern with a marked enrichment in MREE compared to LREE and HREE (Fig. 11B). In the zoisite eclogites, the REE contents of omphacite are very low, mostly below the detection limit (Fig. 11B, Table 1). Omphacite typically has high Li concentrations (100–200 µg/g, Fig. 12B, Table 1). Several other trace elements (B, Pb, Sr, Zr, Hf, Y, Sc) are higher in omphacite from MORB-type eclogites compared to omphacite from zoisite eclogites (Fig. 12B, Table 1). Omphacite grains containing clusters with densely packed fluid inclusions offer the possibility to get information about the trace elements contained in the fluid inclusions. Therefore, fluid inclusion-rich clusters within the omphacite core and inclusion-free parts of the same omphacite grains were analyzed. The comparison of the analyses shows that, considering the error of the trace-element analyses, the elements B, Pb, Ba, Rb, Sr, Sc and Y are significantly higher in the fluid inclusion-bearing core compared to the inclusion-free parts of the grain (Fig. 12C, Table 1).

7. Discussion

7.1 Metamorphic evolution and evidence for fluid flow during eclogite-facies metamorphism

The metamorphic evolution of the Raspas eclogites and their relation to the zoisite veins can be deduced from the petrological studies. Evidence for the prograde metamorphic development in the MORB-type eclogites and zoisite eclogites is given by prograde zoning and mineral inclusions in garnet porphyroblasts. In MORB-type eclogites, decreasing X_{Fe} and spessartine component indicate increasing temperature and the inclusion succession from albite to omphacite from core to rim indicate increasing pressure during garnet growth. Glaucophane inclusions as evidence for prograde blueschist conditions have not been found in eclogites, but prograde blueschists, cofacial to the eclogites, are common in the Raspas Complex and developed from more alkaline precursor rocks with lower X_{Fe} and higher Al_2O_3 contents (John et al., 2010). Garnet in zoisite eclogite is distinguished from that in MORB-type eclogite by a grossular- and X_{Mg}-rich outer rim (Rim 2). Garnet growth during increasing pressure is confirmed for the zoisite eclogites also by the inclusion sequence, from albite and quartz inclusions in the core, omphacite and albite in Rim 1, to omphacite and zoisite in Rim 2. This outer Rim 2 continued to grow under eclogite-facies conditions (Fig. 10). Prograde zoning in omphacite of the zoisite eclogites is also documented by high jadeite contents in strained and recrystallized marginal parts of the grains.

Evidence for the composition of the fluid phase presumably present at the prograde stage is provided in the zoisite eclogites by graphite inclusions in garnet cores. The garnet core grew in the stability field of graphite, presumably in the presence of a fluid phase consisting of H_2O and CH_4. Such a fluid can develop during hydrothermal alteration of the slab in the early stage of subduction due to water percolation through bending-related faults (Mével, 2003; Ranero et al., 2003). Hydrothermal alteration of the precursor rocks of the eclogites is suggested by trace-element (see Section 7.4) and Sr-O isotope data (Halama et al., 2011). During hydrothermal alteration, H_2O and CO_2 will be present while serpentinization of olivine in the basalt or underlying peridotite will supply CH_4 according the reactions:

(1) Olivine + H_2O $\rightarrow$ serpentine + magnetite + H_2

(2) $4H_2 + CO_2 \rightarrow CH_4 + 2H_2O$

Mixing of an H_2O-CO_2 fluid with an H_2O-CH_4 fluid should lead to the precipitation of graphite during subduction (cf. Ferry and Baumgartner, 1987). Increasing pressure at stagnant low temperature extends the graphite stability field up to very near the H_2O-CO_2 and the H_2O-CH_4 tie lines in the C-O-H system (Ferry and Baumgartner, 1987) increasing the probability of graphite precipitation even at low CH_4 contents in the fluid. Increasing temperature at a later stage of subduction then decreases the graphite stability field. This may result in graphite dissolution according to the reaction:

(3) $2C + 2H_2O \rightarrow CH_4 + CO_2$.

Infiltration by an H_2O-rich fluid drives the reaction to the right side. Frequent ankerite inclusions in Rim 1 surrounding the graphite-rich garnet core in the zoisite eclogites suggest that the aqueous fluid invaded the outer part of the garnet, dissolved the graphite, and produced CO_2 which reacted to form ankerite. The required Ca, Mg and Fe cations are supplied either by the aqueous fluid or dissolved from the garnet. A patchy appearance of the outer part of the garnet core, displayed in X-ray maps (Fig. 4B), confirms fluid-induced compositional changes of the garnet. The remaining fluid will be enriched in methane produced by reaction (3). Although the methane will be highly diluted by H_2O infiltration, methane-bearing fluid inclusions could be entrapped in the garnet.

In the zoisite eclogites, omphacite with low jadeite content (about 30% Jd) is partially replaced by omphacite with high jadeite content (45% Jd), resulting in the compositionally patchy texture, probably initiated by fluid infiltration from the veins. The fine-scale patchy variations in jadeite content in omphacite (Fig. 4B) with fluid-filled cavities can be explained by fluid-induced dissolution-precipitation processes (Putnis, 2002; Putnis and John, 2010). In contrast, omphacite in the MORB-type eclogites are rather homogeneous in composition and lack fluid inclusions, thus texturally showing no indication of reequilibration due to metasomatic fluid-mineral interaction.

Evidence for fluid flow along veins deeper in the subduction zone is provided by the occurrence of numerous zoisite veins associated with the zoisite eclogites. The zoisite veins are not formed prior to subduction because they cut the schistosity of the eclogites discordantly. They are also not formed during a late retrograde stage because they are themselves deformed and coexist with the prograde peak-assemblage garnet + omphacite in the reaction zones along the veins. This finding is confirmed by the broken edge of garnet, which was cut by a zoisite vein (Fig. 4C) and is overgrown by the eclogite-facies grossular-rich Rim 2, which itselfs contains omphacite inclusions. High-pressure zoisite-rich veins reported from other localities, which are compositionally more complex, have been interpreted as crystallization products from melts (e.g. Liebscher et al., 2007). However, the nearly monomineralic character of the Raspas zoisite veins argues for a vein formation from a fluid phase. Crystallization from a transitional solute-rich fluid or hydrous melt would result in a more complex association of vein minerals and would necessitate significantly higher pressure/temperature conditions (Kessel et al., 2005). The observation of sector and oscillatory zoning for Sr and Fe (Fig. 3) as well as the highly variable Th, U and LREE within single zoisite grains in the veins (Table 1, SEC31-2-1, Analyses 20, 21) support fast growth in a fluid phase and fluctuations in fluid flux and/or element supply. Similar strong trace-element zonation for Sr, Th and U in zoisite of eclogites from the Trescolmen, central Alps, is interpreted by Zack et al. (2002) to result from episodic fluid infiltration. A strong influx of metasomatizing fluids at peak-metamorphic conditions from the veins into the wall rock eclogites is indicated by the occurrence of sector-zoned zoisite grains even in the eclogite matrix near to the zoisite veins and by oscillatory Ca zoning observed in Rim 2 of garnet (Fig. 4A).

Some zoisite veins contain interstitial albite which might be formed later during uplift. However, according to Wayte et al. (1989), the assemblage zoisite+albite is stable up to about 1.6 GPa at 600°C. During uplift of the eclogites, omphacite is locally replaced by a network of albite veinlets and by poikiloblastic magnesio-hornblende. The amphibole composition suggests a rather steep uplift path in the temperature range of 500-600°C (Fig. 10). Later cooling of the rocks is documented by veins containing albite, actinolite, epidote, chlorite and calcite.

7.2 Fluid inclusion formation

The fluid inclusion textures in the eclogite-facies minerals suggest a primary origin for the majority of fluid inclusions. Due to the absence of trail-bound inclusions transsecting grain boundaries, a late secondary origin can be excluded. The time of fluid inclusion entrapment can be deduced from petrological evidence.

In garnet, scattered fluid inclusions are trapped in the grossular-rich rim formed near the peak of eclogite metamorphism in response to fluid infiltration emanating from the zoisite veins. Thus, the inclusions are regarded as primary formations related to fluid infiltration. Fluid inclusions in zoisite from veins and from zoisite eclogites are dispersed throughout the crystals also indicating a primary origin and thus an entrapment of vein forming fluids. The fluid inclusion clusters frequently observed in the core of large omphacite grains (Fig. 6) argue for a primary origin of the fluid inclusions at the time of the omphacite growth. Similar fluid inclusion distributions in omphacite found in other eclogite-facies terranes have been interpreted as primary features (Gao and Klemd, 2001; Scambelluri et al., 1998; Vallis and Scambelluri, 1996; Giaramita and Sorensen, 1994). The compositionally patchy texture of omphacite in the zoisite eclogite of the Raspas Complex, interpreted to result from dissolution/precipitation processes (see chapter 7.1), is consistent with a fluid inclusion formation connected to this process, since such replacement processes generally result in the development of porosity (Putnis and John, 2010). Accordingly, primary fluid inclusions in omphacite could have been formed during replacement of early omphacite with low jadeite content by omphacite with higher jadeite content, likely at peak metamorphism. Since these fluid inclusions have not been found in the retrogressed parts of the omphacite where albite veinlets and diopside-rich rims occur, a late retrograde formation and fluid infiltration can be excluded. The observed elongated fluid inclusions oriented parallel to the c axis, i.e. to the cleavage intersection of the omphacite crystal, is in accordance with a “crystallographically oriented dissolution-reprecipitation mechanism” (Putnis, 2002), which is the typical mechanism of omphacite formation during eclogitization (John and Schenk, 2003; Putnis and John, 2010). This model is in accordance with older suggestions by Roedder (1984) that replacement reactions might be the cause for fluid inclusion formation. The patchy omphacite texture and the rather homogeneous fluid inclusion composition thus suggest a fluid inclusion formation by replacement processes due to pervasive fluid infiltration.

In the antigorite-chlorite peridotite, the occurrence of tiny fluid inclusions in the neoblastic diopside grains indicates fluid entrapment during high-pressure metamorphism in the subducted slab. Alternating layers of chlorite peridotite additionally containing either antigorite or tremolite depending on slightly different bulk composition, suggest partial dehydration of the ultramafic rocks during high-pressure metamorphism.

Although the textural evidence suggests only one generation of primary fluid inclusions trapped in different eclogite-facies minerals, the position of the isochores in *P–T* space (Fig. 10) is too low for a high-pressure formation. Fluid inclusions in high-grade metamorphic rocks are often subject to reequilibration processes. Abundant experimental evidence was presented in literature that documents compositional and density changes of synthetic and natural fluid inclusions in quartz (e.g. Sterner and Bodnar, 1989; Bakker and Jansen, 1990) at metamorphic conditions. The *P-T-t* path of the eclogite-facies rocks in this study will typically cause extreme overpressures in fluid inclusions that are formed at peak metamorphic conditions. Assuming that omphacite, garnet and zoisite behave similar to quartz, inclusions may reequilibrate to lower densities at lower pressures by decrepitation or fluid diffusion. A similar misfit between fluid inclusion isochores and peak *P-T* conditions is reported from other eclogite-facies terranes (e.g., Philippot and Selverstone, 1991; Klemd et al., 1992; Selverstone et al., 1992).

7.3 Fluid composition: evidence from fluid inclusions

Primary fluid inclusions found in garnet, omphacite and zoisite trapped the fluid present at depths of 60-70 km during eclogite metamorphism and formation of the zoisite veins. In all minerals, the fluid inclusions contain an aqueous low-salinity fluid (mean salinity 2 eq mass% NaCl) with minor CH_4 (~1 mol%) and frequently small calcite crystals.

The post-entrapment modification of the fluid inclusions leading to their density reduction arises the question whether the original fluid composition could still be estimated. Stretching is a modification process, which results in a volume change of the fluid inclusions preserving the fluid composition at the time of trapping (Sterner and Bodnar, 1989; Vityk and Bodnar, 1995). Decrepitation of fluid inclusions and stress-induced hydrolyses of lattice defects and microcracks, in contrast, would remove H_2O from the fluid inclusions increasing the salinity of the fluid (Hollister 1990; Bakker and Jansen 1991, 1994; Johnson and Hollister 1995). However, a significant H_2O loss is unrealistic considering the generally low salinity of the fluid inclusions in the zoisite eclogites and veins. Furthermore, the ratios of major and trace element cations remain basically unchanged (Audétat and Günther, 1999). Another possible modification process is the hydrogen movement into or out of fluid inclusions resulting in fO_2 conditions which do not represent the trapping conditions (Hall and Bodnar, 1990; Mavrogenes and Bodnar, 1994). For rocks buffered at fO_2 near the fayalite-magnetite-quartz equilibrium most uplift paths result in external H_2 overpressures and H_2 movement into the fluid inclusions (Hall and Bodnar, 1990). However, for T-convex uplift paths like that in the Raspas Complex, overpressures calculated by these authors are low. Furthermore, H_2 supply often occurs locally where redox reactions take place (Potter et al., 2004). In this case, H_2 diffusion into an original CO_2-H_2O fluid inclusion will produce CH_4. However in the Raspas eclogites, there is no evidence for such reactions to take place after the entrapment of the fluid inclusions and thus H_2 diffusion is not a significant modification process. The small CH_4 inclusions observed among the dominant aqueous inclusions in zoisite from the veins could be formed by "necking down" (Roedder, 1984) of CH_4-bearing aqueous inclusions after exsolution of a CH_4 vapour phase at temperatures below about 400°C (Holloway, 1984).

Due to the low salinity, the fluid inclusions have the potential to represent the original composition of an infiltrating fluid. In contrast, highly saline fluid inclusions, abundant in other high-pressure terranes, are generally considered to be residues of aqueous fluid–rock interaction or vein formation where H_2O has been consumed by the crystallization of hydrous minerals or by melt formation (Kullerud, 1996; Scambelluri et al., 1998; Hermann et al., 2006). The occurrence of methane in all fluid inclusions is unusual compared to fluid compositions from other eclogite complexes. Other CH_4-bearing aqueous fluid inclusions are known only from eclogites of the Dabie-Sulu terrane of eastern China, Fu et al. (2003). The CH_4-bearing aqueous fluid in low-temperature eclogites is in contrast to CO_2-rich fluid compositions reported from high-temperature eclogites or eclogites, which passed through a granulite stage during uplift, as in the Usagaran belt (Herms, 2002).

Although CO_2 has not been detected by Raman spectroscopy, the occurrence of calcite in the fluid inclusions suggests the presence of CO_2 in the original high-pressure fluid. The common occurrence of calcite in the fluid inclusions disagrees with the assumption of accidentally trapped crystals, particularly since calcite is deficient in the eclogite-facies assemblage and in zoisite veins. Calcite grains inside the fluid inclusions cannot be daughter crystals precipitated from a Ca-containing fluid due to the variable volumetric proportions (5-30%, mean 10%). Instead, they are retrograde reaction products formed between a CO_2-bearing fluid and Ca-rich host minerals. A simple calculation shows that a mixture consisting of 10 vol% calcite and 90 vol% H_2O fluid (density about 1 g/cm^3) contains only about 2.5 mol% CO_2. In fact, during reaction of a CO_2-bearing aqueous fluid with a silicate host mineral, hydroxyl-bearing silicate minerals should form beside carbonate (Kleinefeld and Bakker, 2002). However, the crystallisation of silicates inside the fluid inclusions often is hindered kinetically (Kleinefeld and Bakker, 2002) because of incongruent dissolution of the host mineral.

Molina and Poli (2000) demonstrate by mass-balance and thermodynamic calculations that, in synthetic eclogites of basaltic composition, an H_2O-rich fluid (X_{CO_2}<0.05) coexists with carbonate at 1.6–2.0 GPa below 700°C. The presence of zoisite in eclogites and veins also suggests low X_{CO_2} conditions as discussed by Klemd (2004). The primary aqueous fluid in the Raspas Complex should thus have contained both low CO_2 and low CH_4 contents. Such a fluid composition could evolve from deserpentinization as discussed in Section 7.5. On the other hand, CO_2 and CH_4 may be produced by reaction of an aqueous fluid with graphite-containing metapelites. H_2O-rich fluids with about equal amounts of CO_2 and CH_4 develop during dehydration of graphite-containing rocks at high pressure (>1 GPa) and relatively low temperature (600°C), if a fixed H/O ratio of water (2:1) is assumed (Connolly and Cesare, 1993; Huizenga, 2001). At increasing pressures and lower temperatures, X_{H_2O} increases whereas CO_2 and CH_4 decrease. The amount of CH_4 generally depends on the oxygen fugacity in the rocks. However, the oxygen fugacity is probably controlled by the external aqueous fluid in the metasomatized eclogites and zoisite veins of the Raspas Complex since oxygen-isotope analyses of eclogite minerals indicate disequilibria between garnet and zoisite and between garnet and omphacite (Halama et al., 2011).

7.4 Geochemical evidence for element transfer and metasomatism

The preceding discussion clearly shows that the zoisite eclogites were affected by fluid infiltration related to the zoisite veins. Before attempting to obtain information about element transfer and metasomatism caused by this fluid event, we will consider whether the difference in chemical composition could reflect a protolith difference between the MORB-type and the zoisite eclogites. Major and trace-element compositions of MORB-type eclogites, zoisite eclogites and a zoisite vein are given by John et al. (2010) and Halama et al. (2010). The MORB-type eclogites have been identified by their specific immobile element and REE spectra (Fig. 13A; John et al. 2010). The zoisite eclogites are basaltic with respect to major elements, but are enriched in incompatible trace elements (LREE, MREE, Pb, Sr, Th, U and HFSE) relative to the MORB-type eclogites (Fig. 13A,B). An alkali basaltic protolith to explain elevated LREE content of the zoisite eclogites can be ruled out because of low K, Rb, Ba and Sr compared to LREE contents which are even higher than in alkali basalts. High Sb contents in the zoisite eclogites, like in MORB-type eclogites and serpentinized ultramafic rocks (Fig. 14; for trace-element analyses see John et al., 2010), provide evidence for seafloor alteration in all precursor rocks, consistent with O and Sr isotopic signatures of the MORB-type eclogites (Halama et al., 2011). Thus, seafloor-altered basalts should also have been the precursor rocks for the zoisite eclogites. The close association of MORB-type eclogites and zoisite eclogites invariably occurring together with zoisite veins supports similar protolith compositions. Homogeneous O, Sr and Nd isotopic composition in zoisite eclogites, similar to that of the associated zoisite veins, indicates a significant pervasive fluid overprint (Halama et al., 2011). Similarly, the narrow range of LILE concentrations in the zoisite eclogites is explained by buffering of these fluid-mobile elements by an external fluid, whereas the seafloor-altered MORB-type eclogites have preserved their large variation in LILE contents (Fig. 13B).

The elements Th, U and LREE which are considered as fluid-immobile or less fluid-mobile (Plank, 2005; Hermann et al., 2006) should have been highly mobile in the zoisite vein fluid in the Raspas Complex, because these elements display large variations within single zoisite grains of the veins, probably correlated with oscillatory zoning. Applying the distribution coefficients of Feinemann et al. (2007) to Th, U and La contents in the vein zoisite (Table 1, SEC31-2-1, Analysis 21) predicts equilibrium fluid concentrations of 20 µg/g Th, 7 µg/g U and 94 µg/g La, which are distinctly higher than those determined experimentally at 600 and 650°C from synthetic pelite starting material by Spandler et al. (2007). Such high concentrations in the fluid could explain the high Th and LREE contents in the metasomatized zoisite eclogites. Experimental studies of the stability relations between fluorapatite, allanite and REE-epidote in the presence of different fluid compositions at 450 to 610 MPa and 450 to 500°C show that a high Ca-activity in the fluid promotes monazite dissolution and mobilization of REE and Th (Budzyn et al., 2011). REE-epidote, zoisite or allanite are stabilized in such Ca-rich fluids and could be precipitated in veins like the REE- and Th-rich zoisite of the Raspas veins.

The enrichment of Nb, Ta, Zr and Hf in the zoisite eclogites (Fig. 13) demonstrates the fluid mobility of these elements. HFSE mobility has also been shown in eclogites from other localities (Gao et al., 2007; Spandler et al., 2011). Experimental studies by Rapp et al. (2010) reveal a strongly enhanced solubility of rutile and thus HFSE mobility in chloride and fluoride-bearing hydrous fluids which are stable in the absence of Cl,F-apatite. Berger et al. (2010) report zoisite eclogites from the Limousin area, which are high in HFSE as well as LREE and Sr similar to the Raspas zoisite eclogites. They suggest a metasomatic formation of the zoisite eclogites by channelled fluid-rock interaction at UHP conditions. Although the HFSE are enriched in the Raspas zoisite eclogites, they are low in the zoisite vein (Fig. 13) and the zoisite crystals (Fig. 12). This might be explained by high rutile/fluid distribution coefficients (Brenan et al., 1994) leading to HFSE depletion of the fluid infiltrating the rutile-bearing eclogites. Inside the zoisite veins, rutile did not nucleate, probably because of a low nucleation rate. The occurrence of very large but rare rutile crystals in eclogite-facies veins of the Monviso meta-ophiolite (Spandler et al., 2011) also suggests a low nucleation rate versus growth rate of rutile in high-pressure aqueous fluids.

The extremely low LREE contents of omphacite in the zoisite eclogites, which are quite distinct from those of omphacite from MORB-type eclogites (Fig. 11B), most probably result from equilibration with zoisite during fluid-rock interaction. Zoisite apparently is acting as a sink for these elements because of very high zoisite/clinopyroxene distribution coefficients (e.g. $D^{zoi/cpx}$ = 8510 for Nd; Zack et al., 2002). The fluid-mediated equilibration of omphacite with zoisite most likely occurred by a dissolution-precipitation mechanism (Putnis and John, 2010). This concept is supported by oxygen isotopic mineral studies by Halama et al. (2011) showing equilibration of zoisite with omphacite but not with garnet, which is demonstrated by disequilibrium O isotope composition and the chemical zoning pattern of garnet (Fig. 3).

Direct evidence for the trace-element composition of the metasomatizing fluid has been obtained from the primary fluid inclusions, which can be regarded as remnants of the infiltrating fluid. Laser-ablation ICP-MS analyses of fluid inclusion-rich domains in omphacite from the zoisite eclogite are enriched in the fluid-mobile trace elements B, Rb, Pb, Sr and Sc compared with inclusion-free domains in the same grains (Fig. 12C). Although Sr and Pb could have fractionated into the coexisting zoisite, the fluid is still high in these elements. The elevated content in the immobile and compatible element Sc is not yet understood. A similar study by Hermann et al. (2006) has shown that fluid inclusion-rich omphacite domains in an eclogite-facies vein from Monviso are enriched in Cs, Rb, Ba, Pb, Th, and U.

The major elements Ca, Al, Mg and Si should also have been transported in the fluid, since Ca, Al are enriched, and Mg, Si are deficient in the zoisite eclogites compared to the MORB-type eclogites (for analytical data see Halama et al., 2010, and John et al., 2010). According to Manning (2004), subduction zone fluids in equilibrium with oceanic crust at depths of about 25–50 km, though solute-poor, are relatively enriched in Ca, Al, Na and Si, over Fe and Mg. The solubility of Al at high pressures and temperatures is due to the ability of alkali-alumosilicate components to form polymers (Manning, 2004). High Al contents in the fluid are also found in veins from eclogites at other localities (Becker et al., 1999; John and Schenk, 2003; Gao at al., 2007).

7.5 Origin of the fluid and the sources of the trace elements

The relatively homogeneous composition of fluid inclusions within different minerals of zoisite eclogites and veins are evidence for an open-system fluid infiltration at high flux where the fluid composition is controlled by an external source (e.g., Giaramita and Sorensen, 1994). Evidence for a pervasive, metasomatic fluid overprint along the veins includes homogeneous O, Sr and Nd isotopic compositions of the zoisite eclogites (Halama et al., 2011) and high trace-element concentration (REE, Pb, Sr, Th, U) in the zoisite eclogites adjacent to the veins, relative to the MORB-type eclogites (Fig. 13). In contrast, small-scale fluid flow from internal, rock-buffered in-situ fluid release should produce small-scale fluid-inclusion heterogeneity (e.g. Philippot and Selverstone, 1991), is unlikely to overprint precursor isotopic signals (e.g., Raspas MORB-type eclogites with magmatic Nd and seawater Sr; Halama et al., 2011).

The metasomatizing fluid in the zoisite eclogites of the Raspas Complex could be derived from three possible external sources: dehydration of serpentinites, metasediments, and metabasites located beneath the zoisite eclogites. Variably serpentinized peridotites and metapelites are associated with the eclogites in the Raspas Complex. Modeling by Rüpke et al. (2002) shows that the dehydration of a serpentinized mantle with 5.5 mass% initial H_2O results in about 4 mass% H_2O released at 60 km depth and 550–650°C, similar to estimates of water released (3 mass%) from serpentinized lherzolite at the same *P*–*T* conditions in experiments by Schmidt and Poli (2003). In contrast, only about 1 mass% H_2O is released from metapelites in the temperature range of the blueschist to eclogite-facies transition (Rüpke et al., 2002; Spandler et al., 2003). Additionally, the proportion of sediments in the subducting slab is small compared to the serpentinized slab mantle. Only about 0.5 mass% H_2O could be released from metabasites at temperatures above 650°C in a lower crustal level (Rüpke et al., 2002). From the Münchberg Massif, Liebscher et al., (2007) report a fluid release during crystallization of leuco-tonalitic melt produced by eclogite partial melting at high *P*–*T* conditions (680–750°C, 2.3–3.1 GPa). Such an alternative aqueous fluid source can be ruled out for the Raspas Complex because these authors show that that fluid is sequestered by hydration of the eclogite-facies assemblages near the veins, not affecting the bulk trace-element budget.

In conclusion, a serpentinitic fluid source is most likely to generate a high fluid flow sufficient to infiltrate and metasomatize the mafic oceanic crust. This assumption is particularly relevant to the Raspas Complex, where the eclogites are associated with large volumes of serpentinites (Fig. 1), likely constituting the dominant fluid source. In addition to the common antigorite-chlorite peridotite, deserpentinized tremolite-chlorite peridotite and chlorite harzburgite also occur. The latter, characterized by large radiating orthopyroxene rods (Fig. 5), olivine, chlorite with prograde Cr zoning, and tremolite, greatly resembles the high-pressure dehydration-related chlorite harzburgites with pseudo-spinifex texture from the Almirez Massif (Trommsdorff et al., 1998; Puga et al., 1999; Lopez Sanchez-Vizcaino et al., 2005), which equilibrated at 680 to 710°C and 1.6 to 1.9 GPa (Padron-Navarta et al., 2010). Since the chlorite harzburgites of the Raspas Complex contain the same mineral assemblage as the Almirez harzburgites, the rocks equilibrated in a similar *P-T* range as the Raspas eclogites (Fig. 10, John et al., 2010). Furthermore, the very low Al content of orthopyroxene in the Raspas Complex (0.03-0.10 mass% Al_2O_3), as in the Almirez Massif (<0.5 mass% Al_2O_3, Trommsdorff et al., 1998), is distinct from that of mantle orthopyroxene and is thus a strong indication of formation during high-pressure deserpentinisation (Padron-Navarta et al., 2010). The characteristic pseudo-spinifex texture with fan-shaped orthopyroxene aggregates is the result of fast crystallization after overstepping of the antigorite-breakdown reaction leading to local fluid overpressure, hydraulic fracturing and fluid pulses (Padron-Navarta et al., 2011). In the Raspas Complex, cyclic fluid expulsion is documented by the oscillatory zoning in vein zoisite and garnet rims in the metasomatized eclogites.

The low-salinity aqueous composition of fluid inclusions in the metasomatized eclogites and zoisite veins (0.4–5.3 eq mass% NaCl) is similar to the composition of the fluid released by antigorite breakdown as obtained by Scambelluri et al. (2004a) from mass-balance calculations (0.4–2.0 eq mass% NaCl). The fluid released by deserpentinization may contain methane produced by carbonate reduction in the mantle. Scott et al. (2004) obtained significant CH_4 but negligible CO_2 by experimental carbonate reduction at 500°C and 1-2 GPa. In the Raspas Complex, thus produced CH_4 appears to be trapped in fluid inclusions in clinopyroxene recrystallized during high-pressure metamorphism.

Serpentinization of ultramafic rocks is accompanied by enrichments in fluid-mobile trace elements (B, Cl, Cs, Rb, Ba, Pb, Sr, As and Sb) (Hattori and Guillot, 2003; Tenthorey und Hermann, 2004). Conversely, experimental and fluid inclusion studies show that antigorite breakdown liberates B, As, Cs, Pb, Li, Ba, Be, Rb, U, Sr into the released aqueous fluid (Tenthorey and Hermann, 2004; Scambelluri et al., 2004a, 2004b), although this process alone is unlikely to efficiently metasomatize the mantle wedge to produce the “arc signature” due to the low initial concentrations of most of these elements in serpentinite. In the Raspas Complex, serpentinized peridotites are enriched in Cs, Rb, Ba, Pb, Sb and W relative to depleted mantle (John et al., 2010), but fluid-mobile trace elements occur in similar concentrations in both deserpentinized chlorite harzburgite and serpentinitic rocks (Fig. 14), which is also the case for serpentinized and deserpentinized rocks of the Almirez Massif (Garrido et al., 2005). Thus, while deserpentinization might mobilize a range of trace elements, their concentration in the fluid is low and most trace elements may be immediately bound to reaction products like pyroxene and amphibole.

The serpentinites probably act primarily as a source for H_2O-rich but trace-element poor fluids which may, during migration through the lithosphere, leach solutes from overlying metabasites or metapelites. The liberation of trace elements is achieved primarily by dissolution-precipitation reactions in zones of intense fluid-rock interaction at high fluid fluxes (Bebout and Barton, 1993; John et al., 2008; Zack and John, 2007; Putnis and John, 2010). Such zones of intense fluid-rock interaction might form along pathways of slab-fluid escape where the permeability of the rock, induced by hydraulic fracturing, is enhanced by a high fluid flow (John et al., 2008; Beinlich et al., 2010). The duration of fluid flow and reaction time should be on the same time-scale to allow significant mineral reactions and mass exchange to occur. The dissolved trace elements will be transported to zones of lower fluid pressure and temperature where they can be incorporated in vein minerals, fixed in the infiltrated wall rock, or leave the slab to metasomatize the mantle wedge.

A favourable candidate for a rock that has interacted with external, serpentinite-derived fluids is the garnet-amphibole rock (Sample SEC13-1). Compared to MORB, this rock is deficient in LREE, MREE and Sr, which are enriched in the metasomatized zoisite eclogites (Fig. 13A,B). The significant LREE and MREE depletion of the garnet-amphibole rock compared to MORB-type eclogites (Fig. 13A) causes an unusual "step-shaped" REE pattern, which does not resemble the REE pattern of present-day unmetamorphosed igneous rocks (Bernard-Griffiths et al., 1991). That pattern is interpreted to indicate that LREE were flushed out under open-system conditions. John et al. (2004) found a similar trace-element pattern for some Zambian eclogites where LREE are depleted relative to the immobile HREE and HFSE due to intense fluid-rock interaction at high fluid flux.

Enriched Th and U in the zoisite eclogites of the Raspas Complex cannot be derived from leaching of metabasites only, considering the low Th and U content of these rocks. Subducted sediments are the main source of Th and U as well as LILE to arc rocks (Plank and Langmuir, 1998). The high Th and U contents in the vein fluid (predicted for vein zoisite by inverting the distribution coefficients by Feinemann et al., 2007) suggest that these elements have been mobile and were transported in the fluid. Monazite in the metapelites could be the source of Th, U and REE, if Ca-rich fluids locally dissolved the monazite (Budzyn et al., 2011). The Raspas metapelites are in part metasomatized by Ca-rich fluids suggested from the occurrence of schists rich in Ca-amphibole and epidote, additionally containing relict kyanite. Sr and Nd data from the Raspas zoisite eclogites (initial $^{87}Sr/^{86}Sr$ = 0.7075-0.7081, εNd_{130Ma} = -6.7 to -8.7) indicate a sediment contribution (Halama et al. (2011), so the aqueous fluid derived from the serpentinites possibly leached Th, U, and Sr from the metasediments intercalated in the eclogite suite. If the aqueous fluid reacted with graphite-bearing metapelites, about equal amounts of CO_2 and CH_4 should have been produced (as discussed in Section 7.3). At present, we are not able to decide whether methane and CO_2 originate from mantle rocks or from metapelites.

In summary, we can conclude that the fluids mainly derived from dehydrating serpentinites and that some elements enriched in the zoisite eclogites were derived from leaching the metabasites (Ca, Sr, LREE and MREE) and others were derived from leaching metasediments (Th, U). Most of the elements (Th, U, LILE and LREE) enriched in the zoisite eclogites and in the zoisite veins of the Raspas Complex are typically enriched in arc magmas suggesting that at least some are transported by channelized fluid flow further into the mantle wedge where arc magmas are generated.

8. Conclusions

(1) In the Raspas Complex, MORB-type eclogites occur alongside zoisite eclogites, which are associated with monomineralic zoisite veins. Petrologic studies show that zoisite veins formed from the fluid phase at high-pressure conditions.

(2) A homogeneous H_2O-rich fluid composition with low salinity and minor amounts of CO_2 and CH_4, suggested from the study of fluid inclusions in zoisite eclogites and veins, gives evidence for external fluid supply. Oscillatory zoning in zoisite and garnet of zoisite eclogites associated with the veins indicates fluid fluctuations and fluid infiltration into the eclogites. Deserpentinized ultramafitites are potential source rocks for the aqueous fluid. The pseudo-spinifex texture observed in chlorite harzburgites suggests fast growth of orthopyroxene after overstepping of antigorite breakdown leading to local fluid overpressure, hydraulic fracturing and fluid pulses.

(3) Compared to the MORB-type eclogites, the zoisite eclogites and zoisite veins are enriched in LREE, MREE, Pb, Sr, Th, U, indicating that all these elements were mobile in the metasomatizing fluid. The elements Th, U and LREE, which are considered as less fluid-mobile, should have been highly mobile in the vein-forming fluid, because these elements display large variations within single zoisite grains. In addition, the fluid-mobile trace elements B, Rb, Pb, Sr are found in fluid inclusions in omphacite.

(4) Channelized fluid flow from a serpentinitic mantle source can explain the low-salinity aqueous fluid composition but not the high trace element concentrations in the metasomatized zoisite eclogites and zoisite veins. Trace elements are probably leached from metabasites and metapelites in zones of intense fluid-rock interaction. A garnet-amphibole rock seems to represent such a leached rock, which is deficient in LREE, MREE and Sr, i.e., trace elements enriched in the zoisite eclogites. On the other hand, the fluid-mobile LILE and B are likely derived from metapelites intercalated in the eclogite suite. The less fluid-mobile elements Th and U, which display extremely variable concentrations in vein zoisite, could also be supplied from the metapelites.

(5) The case study in the Raspas Complex, Ecuador, has shown that a large range of trace elements (B, LILE, LREE, MREE, Th, U) are fluid-mobile under eclogite-facies conditions and may be transported by channelized fluid flow and high fluid flux into the mantle wedge, where arc magmas are generated.

Acknowledgements

This publication is contribution no. 172 of the Sonderforschungsbereich 574 “Volatiles and Fluids in Subduction Zones” at the University of Kiel, supported by the Deutsche Forschungsgemeinschaft. We thank H. Brätz (Würzburg/Erlangen) for assistance at the LA-ICP-MS, B. Mader (Kiel) at the electron microprobe and M. Baumgartner (Leoben, Austria) for the intensive help at the Raman Spectrometer. Sincere thanks go to P. Raase for fruitful discussions and comments and for the internal review. We are indebted to R. Halama and D. Garbe-Schönberg for the geochemical analyses of the harzburgite sample. We thank R. Halama for his careful and constructive review. J. Hermann, T. Pettke and anonymous journal reviewers are thanked for their fruitful critical reviews, which greatly improved the earlier and the latest version of the manuscript. We sincerely thank Erin Todd for his thorough proofreading.

Appendix A. Petrography and mineral chemistry

Appendix B. Supplementary figures

Appendix C. Supplementary data

References

Aspden, J.A., Bonilla, W., Duque, P., 1995. The El Oro metamorphic Complex, Ecuador: geology and economic mineral deposits. British Geological Survey Publications: Nottingham.

Audétat, A., Günther, D., 1999. Mobility and H_2O loss from fluid inclusions in natural quartz crystals. Contrib. Mineral. Petrol. 137, 1-14.

Bakker, R.J., 1997. Clathrates: Computer programs to calculate fluid inclusion V-X properties using clathrate melting temperatures. Computers & Geosciences 23, 1-18.

Bakker, R.J., 2003. Package FLUIDS 1. Computer programs for analysis of fluid inclusion data and for modelling bulk fluid properties. Chem. Geol. 194, 3-23.

Bakker, R.J., Jansen, J.B.H., 1990. Preferential water leakage from fluid inclusions by means of mobile dislocations. Nature 345, 58-60.

Bakker, R.J., Jansen, J.B.H., 1991. Experimental post-entrapment water loss from synthetic CO_2-H_2O inclusions in natural quartz. Geochim. Cosmochim. Acta 55, 2215-2230.

Bakker, R.J., Jansen, J.B.H., 1994. A mechanism for preferential H_2O leakage from fluid inclusions in quartz, based on TEM observations. Contrib. Mineral. Petrol. 116, 7-20.

Bebout, G.E., Barton, M.D., 1993. Metasomatism during subduction: products and possible paths in the Catalina Schist, California. Chem. Geol. (special issue) 108, 61-92.

Becker, H., Jochum, K.P., Carlson, R.W., 1999. Constraints from high-pressure veins in eclogites on the composition of hydrous fluids in subduction zones. Chem. Geol. 160, 291-308.

Beinlich, A., Klemd, R., John, T., Gao, J., 2010. Trace-element mobilization during Ca-metasomatism along a major fluid conduit: eclogitization of blueschist as a consequence of fluid-rock interaction. Geochim. Cosmochim. Acta. 74, 1892-1922.

Berger, J., Féménias, O., Ohnenstetter, D., Bruguier, O., Plissart, G., Mercier, J.-C.C., Demaiffe, D., 2010. New occurrence of UHP eclogites in Limousin (French Massif Central): age, tectonic setting and fluid-rock interactions. Lithos 118, 365-382.

Bernard-Griffiths, J., Peucat, J.-J., Ménot, R.-P., 1991. Isotopic (Rb-Sr, U-Pb and Sm-Nd) and trace element geochemistry of eclogites from the pan-African Belt: A case study of REE fractionation during high-grade metamorphism. Lithos 27, 43-57.

Bosch, D., Gabriele, P., Lapierre, H., Malfere, J.L., Jaillard, E., 2002. Geodynamic significance of the Raspas metamorphic complex (SW Ecuador); geochemical and isotopic constraints. Tectonophysics 345, 83-102.

Boynton W.V., 1984. Geochemistry of the rare earth elements: meteorite studies, in: Henderson, P. (Ed.), Rare earth element geochemistry. Elsevier, Amsterdam, pp. 63-114.

Brenan, J.M., Shaw, H.F., Phinney, D.L., Ryerson, F.J., 1994. Rutile-aqueous fluid partitioning of Nb, Ta, Hf, Zr, U and Th: Implications for high field strength element depletions in island arc basalts. Earth Planet. Sci. Lett. 128, 327-339.

Budzyn, B., Harlov, D.E., Williams, M.L., Jercinovic, M.J., 2011. Experimental determination of the stability relations between monazite, fluorapatite, allanite, and REE-epidote as a function of pressure, temperature, and fluid composition. Am. Mineralogist 96, 1547-1567.

Connolly, J.A.D., Cesare, B., 1993. C-O-H-S fluid composition and oxygen fugacity in graphitic metapelites. J. metamorph. Geol. 11, 379-388.

Elliott, T., 2003. Tracers of the slab, in: Eiler, J. (Ed), Inside the Subduction Factory. Geophys. Mon., vol. 138. American Geophysical Union, Washington, DC, pp. 23-45.

Feineman, M.D., Ryerson, F.J., DePaolo, D.J., Plank, T., 2007. Zoisite-aqueous fluid trace element partitioning with implications for subduction zone fluid copmosition. Chem. Geol. 239, 250-265.

Feininger, T., 1978. Geologic map of western El Oro Province. 1/50000. Escuela Politecnica Nacional, Quito, Ecuador.

Feininger, T., 1980. Eclogite and related high-pressure regional metamorphic rocks from the Andes of Ecuador. J. Petrol. 21, 107-140.

Feininger, T., 1982. The metamorphic “basement” of Ecuador. Geol. Soc. Am. Bull. 93, 87-92.

Feininger, T., 1987. Allochthonous terranes in the Andes of Ecuador and northwestern Peru. Canadian Journal of Earth Sciences 24, 266-278.

Ferry, J.M., Baumgartner, L., 1987. Thermodynamic models of molecular fluids at the elevated pressures and temperatures of crustal metamorphism, in: Carmichael, I.S.E., Eugster, H.P. (Eds), Thermodynamic modeling of geological materials: Minerals, fluids and melts. Mineralogical Society of America, Rev. Mineral. 17, pp. 323-365.

Fu, B., Touret, J.L.R., Zheng, Y.-F., 2003. Remnants of premetamorphic fluid and oxygen isotopic signatures in eclogites and garnet clinopyroxenite from the Dabie-Sulu terranes, eastern China. J. metamorph. Geol. 21, 561-578.

Gabriele, P., 2002. HP terranes exhumation in an active margin setting: geology, petrology and geochemistry of the Raspas Complex in SW Ecuador. Unpublished Ph.D. thesis, University of Lausanne, Switzerland.

Gabriele, P., Ballèvre, M., Jaillard, E., Hernandez, J., 2003. Garnet-chloritoid-kyanite metapelites from the Raspas Complex, SW Ecuador; a key eclogite-facies assemblage. Eur. J. Mineral. 15, 977-989.

Gabriele, P., Piccardo, G.B., Martinotti, G., Hernandez, J., 2002. The high-pressure ultramafic sequence of the El Toro Formation (El Oro Metamorphic Complex, SW Ecuador): Characterization and Metamorphic Evolution. 5th International Symposium on Andean Geodynamics (ISAG). Toulouse, France, (Abstract Volume), pp. 227-230.

Gao, J., John, T., Klemd, R., Xiong, X., 2007. Mobilization of Ti-Nb-Ta during subduction: evidence from rutile-bearing dehydration segregations and veins hosted in eclogite, Tianshan, NW China. Geochim. Cosmochim. Acta 71, 4974-4996.

Gao, J., Klemd, R., 2001. Primary fluids entrapped at blueschist to eclogite transition: evidence from the Tianshan meta-subduction complex in northwestern China. Contrib. Mineral. Petrol. 142, 1-14.

Garbe-Schönberg, C.D., 1993. Simultaneous determination of thirty-seven trace elements in twenty-eight international rock standards by ICP-MS. Geostandards Newsletter 17, 81-97.

Garrido, C.J., López Sánchez-Vizcaíno, V., Gómez-Pugnaire, M.T., Trommsdorff, V., Alard O., Bodinier, JL., Godard, M., 2005. Enrichment of HFSE in chlorite-harzburgite produced by high-pressure dehydration of antigorite-serpentinite: Implications for subduction magmatism. Geochem. Geophys. Geosys. 6(1), Q01J15, doi:10.1029/2004GC000791.

Giaramita, M.J., Sorensen, S.S., 1994. Primary fluids in low-temperature eclogites: evidence from two subduction complexes (Dominican Republic, and California, USA). Contrib. Mineral. Petrol. 117, 279-292.

Halama, R., Bebout, G., John, T., Schenk, V., 2010. Nitrogen recycling in subducted oceanic lithosphere: The record in high- and ultrahigh-pressure metabasaltic rocks. Geochim. Cosmochim. Acta 74, 1636-1652.

Halama, R., John, T., Herms, P., Hauff, F., Schenk, V., 2011. A stable (Li, O) and radiogenic (Sr, Nd) isotope perspective on metasomatic processes in a subducting slab. Chem. Geol. 281, 151-166.

Hall, D.L., Bodnar, R.J., 1990. Methane in fluid inclusions from granulites: A product of hydrogen diffusion? Geochim. Cosmochim. Acta 54, 641-651.

Hattori, K., Guillot, S., 2003. Volcanic fronts form as a consequence of serpentinite dehydration in the forearc mantle wedge. Geology 31, 525-528.

Herms, P., 2002. Fluids in a 2 Ga old subduction zone – deduced from eclogite-facies rocks of the Usagaran belt, Tanzania. Eur. J. Mineral. 14, 361-373.

Hermann, J., Spandler, C., Hack, A., Korsakov, A.V., 2006. Aqueous fluids and hydrous melts in high-pressure and ultra-high pressure rocks: Implications for element transfer in subduction zones. Lithos 92, 399-417.

Hofmann, A.W., 1988. Chemical differentiation of the Earth; the relationship between mantle, continental crust, and oceanic crust. Earth Planet. Sci. Lett. 90, 297-314.

Hollister, L.S., 1990. Enrichment of CO_2 in fluid inclusions in quartz by removal of H_2O during crystal-plastic deformation. J. Struct. Geol. 12, 895-901.

Holloway, J.R., 1984. Graphite-CH_4-H_2O-CO_2 equilibria at low-grade metamorphic conditions. Geology 12, 455-458.

Huizenga, J-M., 2001. Thermodynamic modelling of C-O-H fluids. Lithos 55, 101-114.

John, T., Klemd, R., Gao, J., Garbe-Schönberg, C.D., 2008. Trace-element mobilization in slabs due to non steady-state fluid-rock interaction: constraints from an eclogite-facies transport vein in blueschist (Tianshan, China). Lithos 103, 1-24.

John, T., Schenk, V., 2003. Partial eclogitization of gabbroic rocks in a late Precambrian subduction zone (Zambia): prograde metamorphism triggered by fluid infiltration. Contrib. Mineral. Petrol. 146, 174-191.

John, T., Scherer, E.E., Haase, K., Schenk, V., 2004. Trace element fractionation during fluid-induced eclogitization in a subducting slab: Trace element and Lu-Hf-Sm-Nd isotope systematics. Earth Planet. Sci. Lett. 227, 441-456.

John, T., Scherer, E.E., Schenk, V., Herms, P., Halama, R., Garbe-Schönberg, D., (2010). Subducted seamounts in an eclogite-facies ophiolite sequence: The Andean Raspas Complex, SW Ecuador. Contrib. Mineral. Petrol.. 159, 265-284.

Johnson, E.L., Hollister, L.S., 1995. Syndeformational fluid trapping in quartz: determining the pressure-temperature conditions from fluid inclusions and the formation of pure CO_2 fluid inclusions during grain-boundary migration. J. metamorph. Geol. 13, 239-249.

Kessel, R., Ulmer, P., Pettke, T., Schmidt, M.W., Thompson, A.B., 2005. Trace element signature of subduction-zone fluids, melts and supercritical liquids at 120-180 km depth. Nature 437, 724-727.

Kleinefeld, B., Bakker, R.J., 2002. Fluid inclusions as microchemical systems: evidence and modelling of fluid-host interactions in plagioclase. J. metamorph. Geol. 20, 845-858.

Klemd, R., 2004. Fluid inclusions in epidote minerals and fluid development in epidote-bearing rocks, in: Liebscher, A., Franz, G. (Eds), Epidotes. Mineralogical Society of America, Reviews in Mineralogy and Geochemistry, 56, pp. 197-234.

Klemd, R., van den Kerkhof, A.M., Horn, E.E., 1992. High-density CO_2-N_2 inclusions in eclogite-facies metasediments of the Münchberg gneiss complex, SE Germany. Contrib. Mineral. Petrol. 111, 409-419.

Kroslakova, I., Günther, D., 2007. Elemental fractionation in laser ablation-inductively coupled plasma-mass spectrometry: evidence for mass load induced matrix effects in the ICP during ablation of a silicate glass. J. Anal. At. Spectrom. 22, 51-62.

Kullerud, K., 1996. Chlorine-rich amphiboles ; interplay between amphibole composition and an evolving fluid. Eur. J. Mineral. 8, 355-370.

Liebscher, A., Franz, G., Frei, D., Dulski, P., 2007. High-pressure melting of eclogite and the P-T-X history of tonalitic to trondhjemitic zoisite-pegmatites, Münchberg Massif, Germany. J. Petrol. 48, 1001-1019.

López Sánchez-Vizcaíno, V., Trommsdorff, V., Gómez-Pugnaire, M.T., Garrido, C.J., Müntener, O., Connolly, J.A.D., 2005. Petrology of titanian clinohumite and olivine at the high-pressure breakdown of antigorite serpentinite to chlorite harzburgite (Almirez Massif, S. Spain). Contrib. Mineral. Petrol. 149, 627-646.

Manning, C.E., 2004. The chemistry of subduction-zone fluids. Earth Planet. Sci. Lett. 223, 1-16.

Mavrogenes, J.A., Bodnar, R.J., 1994. Hydrogen movement into and out of fluid inclusions in quartz: experimental evidence and geologic implications. Geochim. Cosmochim. Acta 58, 141-148.

McDonough, W.F., Sun, S.-S., 1995. The composition of the Earth. Chem. Geol. 120, 223-253.

Mével, C., 2003. Serpentinization of abyssal peridotites at mid-ocean ridges. Comptes Rendus Geoscience 335, 825-852.

Molina, J.F., Poli, S., 2000. Carbonate stability and fluid composition in subducted oceanic crust: an experimental study on H_2O-CO_2-bearing basalts. Earth Planet. Sci. Lett. 176, 295-310.

Padrón-Navarta, J.A., Hermann, J., Garrido, C.J., López Sánchez-Vizcaíno, V., Gómez-Pugnaire, M.T., 2010. An experimental investigation of antigorite dehydration in natural silica-enriched serpentinite. Contrib. Mineral. Petrol. 159, 25-42.

Padrón-Navarta, J.A., López Sánchez-Vizcaíno, V., Garrido, C.J., Gómez-Pugnaire, M.T., 2011. Metamorphic record of high-pressure dehydration of antigorite serpentinite to chlorite harzburgite in a subduction setting (Cerro del Almirez, Nevado-Filábride Complex, Southern Spain). J. Petrol. 52, 2047-2078.

Pearce, N.J.G., Perkins, W.T., Westgate, J.A., Gorton, M.P., Jackson, S.E., Neal, C.R., Chenery, S.P., 1997. A compilation of new and published major and trace element data for NIST SRM 610 and NIST SRM 612 glass reference materials. Geostand. Newslett. 21, 115-144.

Philippot, P., Selverstone, J., 1991. Trace-element-rich brines in eclogitic veins: implications for fluid composition and transport during subduction. Contrib. Mineral. Petrol. 106, 417-430.

Plank, T., 2005. Constraints from thorium/lanthanum on sediment recycling at subduction zones and the evolution of the continents. J. Petrol. 46, 921-944.

Plank, T., Langmuir, C.H., 1993. Tracing trace elements from sediment input to volcanic output at subduction zones. Nature 362, 739-743.

Plank, T., Langmuir, C.H., 1998. The chemical composition of subducting sediment: implications for the crust and mantle. Chem. Geol. 145, 325-394.

Potter, J., Rankin, A.H., Treloar, P.J., 2004. Abiogenic Fischer-Tropsch synthesis of hydrocarbons in alkaline igneous rocks; fluid inclusion, textural and isotopic evidence from the Lovozero Complex, N.W. Russia. Lithos 75, 311-330.

Puga, E., Nieto, J.M., Díaz de Federico, A., Bodinier, J.L., Morten, L., 1999. Petrology and metamorphic evolution of ultramafic rocks and dolerite dykes of the Betic Ophiolitic Association (Mulhacén Complex, SE Spain): evidence of eo-Alpine subduction following an ocean-floor metasomatic process. Lithos 49, 23-56.

Putnis, A., 2002. Mineral replacement reactions: from macroscopic observations to microscopic mechanisms. Mineral. Mag. 66, 689-708.

Putnis, A., John, T., 2010. Replacement processes in the Earth’s crust. Elements 6, 159-164.

Ranero, C.R., Morgan, J.P., McIntosh, K., Reichert, C., 2003. Bending-related faulting and mantle serpentinization at the Middle American Trench. Nature 425, 367-373.

Rapp, J.F., Klemme, S., Butler, I.B., Harley, S.L., 2010. Extremely high solubility of rutile in chloride and fluoride-bearing metamorphic fluids: An experimental investigation. Geology 38, 323-326.

Roedder, E., 1984. Fluid inclusions. Mineralogical Society of America, Rev Mineral. 12, pp. 17.

Rüpke, L., Morgan, J.P., Hort, M., Connolly, J.A.D., 2002. Are the regional variations in Central American arc lavas due to differing basaltic versus peridotitic slab sources of fluids? Geology 30, 1035-1038.

Scambelluri, M., Bottazi, P., Trommsdorff, V., Vannucci, R., Hermann, J., Gòmez-Pugnaire, M., Lòpes-Sànchez Vizcaino, V., 2001. Incompatible element-rich fluids released by antigorite breakdown in deeply subducted mantle. Earth Planet. Sci. Lett. 192, 457-470.

Scambelluri, M., Fiebig, J., Malaspina, N., Müntener, O., Pettke, T., 2004a. Serpentinite subduction: Implications for fluid processes and trace-element recycling. International Geology Review 46, 595-613.

Scambelluri, M., Müntener, O., Ottolini, L., Pettke, T.T., Vannucci, R., 2004b. The fate of B, Cl and Li in the subducted oceanic mantle and in the antigorite breakdown fluids. Earth Planet. Sci. Lett. 222, 217-234.

Scambelluri, M., Pennacchioni, G., Philippot, P., 1998. Salt-rich aqueous fluids formed during eclogitization of metabasites in the Alpine continental crust (Austroalpine Mt. Emilius unit, Italian western Alps). Lithos 43, 151-167.

Scambelluri, M., Piccardo, G.B., Philippot, P., Robbiano, A., Negretti, L., 1997. High salinity fluid inclusions formed from recycled seawater in deeply subducted alpine serpentinite. Earth Planet. Sci. Lett. 148, 485-499.

Schmidt, M.W., Poli, S., 1998. Experimentally based water budgets for dehydrating slabs and consequences for arc magma generation. Earth Planet. Sci. Lett. 163, 361-379.

Schmidt, M.W., Poli, S., 2003. Generation of mobile components during subduction of oceanic crust. In: Rudnick, R.L. (Ed.), The Crust, Vol. 3, Treatise on geochemistry (Holland, H.D. and Turekian, K.K., Eds.), Elsevier-Pergamon, Oxford, pp 567-591.

Schulz, B., Klemd, R., Braetz, H., 2006. Host rock compositional controls on zircon trace element signatures in metabasites from the Austroalpine basemant. Geochim. Cosmochim. Acta. 70, 697-710.

Scott, H.P., Hemley, R.J., Mao, H.K., Herschbach, D.R., Fried, L.E., Howard, W.M., Bastea, S., 2004. Generation of methane in the Earth's mantle: in situ high pressure-temperature measurements of carbonate reduction. Proc. Natl. Acad. Sci. U.S.A. 101, 14023-14026.

Selverstone, J., Franz, G., Thomas, S., Getty, S., 1992. Fluid variability in 2 GPa eclogites as an indicator of fluid behavior during subduction. Contrib. Mineral. Petrol. 112, 341-357.

Shi, G.U., Tropper, P., Cui, W., Tan, J., Wang, C., 2005. Methane (CH_4)-bearing fluid inclusions in the Myanmar jadeitite. Geochemical Journal 39, 503-516.

Smye, A.J., Greenwood, L.V., Holland, T.J.B., 2010. Garnet-chloritoid-kyanite assemblages: eclogite facies indicators of subduction constraints in orogenic belts. J. Metam. Geology 28, 753-768.

Spandler, C.J., Hermann, J., Arculus, R.J., Mavrogenes, J.A., 2003. Redistribution of trace elements during prograde metamorphism from lawsonite blueschist to eclogite facies; implications for deep subduction-zone processes. Contrib. Mineral. Petrol. 146, 205-222.

Spandler, C., Hermann, J., Arculus, R., Mavrogenes, J., 2004. Geochemical heterogeneity and element mobility in deeply subducted oceanic crust; insights from high-pressure mafic rocks from New Caledonia. Chem. Geol. 206, 21-42.

Spandler, C., Mavrogenes, J., Hermann, J., 2007. Experimental constraints on element mobility from subducted sediments using high-P synthetic fluid/melt inclusions. Chem. Geol. 239, 228-249.

Spandler, C., Pettke, T., Rubatto, D., 2011. Internal and external fluid sources for eclogite-facies veins in the Monviso meta-ophiolite, Western Alps: implications for fluid flow in subduction zones. J. Petrology 52, 1207-1236.

Sterner, S.M., Bodnar, R.J., 1989. Synthetic fluid inclusions VII. Reequilibration of fluid inclusions in quartz during laboratory-simulated metamorphic burial and uplift. J. metamorph. Geol. 7, 243-260.

Tenthorey, E., Hermann, J., 2004. Composition of fluids during serpentinite breakdown in subduction zones: Evidence for limited boron mobility. Geology 32, 865-868.

Trommsdorff, V., López Sánchez-Vizcaíno, V., Gómez-Pugnaire, M.T., Müntener, O., 1998. High pressure breakdown of antigorite to spinifex-textured olivine and orthopyroxene, SE Spain. Contrib. Mineral. Petrol. 132, 139-148.

Vallis, F., Scambelluri, M., 1996. Redistribution of high-pressure fluids during retrograde metamorphism of eclogite-facies rocks (Voltri Massif, Italian western Alps). Lithos 39, 81-92.

Vielzeuf, D., Baronnet, A., Perchuk, A.L., Laporte, D., Baker, M.B., 2007. Calcium diffusivity in alumino-silicate garnets: an experimental and ATEM study. Contrib. Mineral. Petrol. 154, 153-170.

Vityk, M.O., Bodnar, R.J., 1995. Textural evolution of synthetic fluid inclusions in quartz during reequlibration with application to tectonic reconstruction. Contrib. Mineral. Petrol. 121, 309-323.

Wayte, G.J., Worden, R.H., Rubie, D.C., Droop, G.T.R., 1989. A TEM study of disequilibrium plagioclase breakdown at high pressure: the role of infiltrating fluid. Contrib. Mineral. Petrol. 101, 426-437.

Zack, T., John, T., 2007. An evaluation of reactive fluid flow and trace element mobility in subducting slabs. Chem. Geol. 239, 199-216.

Zack, T., Foley, S.F., Rivers, T., 2002. Equilibrium and disequilibrium trace element partitioning in hydrous eclogites (Trescolmen, Central Alps). J. Petrol. 43, 1947-1974.

Figure captions

Fig. 1. Geological map showing the lithological units of the El Oro Metamorphic Complex, SW Ecuador (modified after Gabriele, 2002). Sample locations are indicated in the enlarged part of the Raspas river profile (lower inset). All sample numbers used in the manuscript have the prefix SEC (South Ecuador) and a suffix indicating the specific sample within an outcrop. Asterisks indicate samples taken from boulders. Location 36 is outside the Raspas river profile. Supplementary unnumbered locations are shown to give some impression about the distribution of rock types.

Fig. 2. Monomineralic zoisite vein (light) cutting the schistosity of the eclogite. Note the deformed contact surface.

Fig. 3. (A,B) X-ray maps for vein zoisite showing oscillatory and sector zoning for Sr and Fe; (C) core-rim compositional profile A–B across the zoisite indicated in (A).

Fig. 4. X-ray maps of a garnet porphyroblast and adjacent omphacite in zoisite eclogite (A,B, Sample SEC29-2A) and of a garnet porphyroblast cut by a zoisite vein, showing the newly grown grossular-rich Rim 2 at the contact (C-E, Sample SEC27-2A).

Fig. 5. Macrophotograph of a polished section of deserpentinized chlorite harzburgite showing large fan-shaped aggregates of orthopyroxene.

Fig. 6. Omphacite with clouded fluid inclusion-rich cores in zoisite eclogite from the Raspas Complex (microphotograph with crossed polarizers).

Fig. 7. Microphotographs of fluid inclusions in (A-D) zoisite eclogites and zoisite veins and (E) antigorite-chlorite peridotite. (A) Calcite-bearing H_2O-NaCl-CH_4 inclusion in a fluid inclusion cluster, elongated parallel c of the omphacite host. (B) H_2O-NaCl-CH_4 fluid inclusion with a calcite lying in Rim 2 of garnet. (C) Fluid inclusions with variable shape dispersed all over a vein zoisite: Among H_2O-NaCl-CH_4 inclusions small, irregular water-free

CH_4 inclusions (see inset) are found, with graphite (black dot) and minor ethane. (D) Elongated H_2O-NaCl-CH_4 fluid inclusion with two calcite crystals and an analcite crystal in omphacite, interpreted as retrograde reaction products. (E) Single small fluid inclusion filled with mixed hydrocarbons in recrystallized clinopyroxene.

Fig. 8. Frequency histograms of (A) melting temperatures (T_m) and (B) homogenization temperatures (T_h) of H_2O-NaCl-CH_4 fluid inclusions in different minerals in the zoisite eclogites and veins.

Fig. 9. Raman spectra of H_2O-rich fluid inclusions (A,C). The laser beam was focussed in the bubble of the two-phase inclusions. (A) Typical Raman spectrum with CH_4 and H_2O peaks for a fluid inclusion in omphacite in zoisite eclogite (time: 60 sec; accumulation: 5 times); (B) Raman spectrum of a water-free CH_4 inclusion (T_h = -90.3°C) in vein zoisite shows graphite and CH_4 peaks (time: 10 sec; accumulation: 5 times); (C) Spectrum showing a CH_4 peak and a peak for structurally bound OH in vein zoisite (time: 10 sec; accumulation: 5 times); (D) Spectrum of a CH_4/hydrocarbon-bearing fluid inclusion in the recrystallized rim of clinopyroxene (Cpx2) in the antigorite-chlorite peridotite; the broad fluorescent shoulder at wavelengths above 3000 cm^{-1} obscures the Raman bands of H_2O (time: 600 sec; accumulation: 2 times).

Fig. 10. *P-T* conditions for the eclogites of the Raspas Complex (John et al., 2010) and assumed *P-T* path, correlated with stages of garnet growth, vein formation, retrograde assemblages and with model isochores for the aqueous inclusions of the highest and lowest salinities, assuming inclusion compositions in the H_2O-NaCl system. For pure methane inclusions, the second most highest and second most lowest homogenization temperatures are selected. The representative isochore for fluid compositions in the H_2O-NaCl-CH_4 system is based on the ice and clathrate-melting temperature determined by Raman spectroscopy.

Fig. 11. Chondrite-normalized (Boynton, 1984) REE pattern of zoisite and omphacite from the Raspas Complex: (A) Zoisite in veins and matrix of eclogites; (B) Omphacite in MORB-type and zoisite eclogites.

Fig. 12. Primitive mantle-normalized (McDonough and Sun, 1995) trace-element contents in zoisite and omphacite from the Raspas Complex: (A) Vein zoisite and matrix zoisite in zoisite eclogites; (B) omphacite in MORB-type and zoisite eclogites; (C) omphacite in zoisite

eclogite comparing fluid inclusion-rich and fluid inclusion-free grain domains (error bar indicates 1-sigma error; base of arrow indicates detection limit).

Fig. 13. (A) Chondrite-normalized (Boynton, 1984) REE concentrations and (B) trace-element contents normalized to N-MORB (Hofmann, 1988) for MORB-type (7 samples) and zoisite eclogites (4 samples), garnet-hornblende rock (SEC13-1), and a zoisite vein. Analytical data for MORB-type eclogites published by John et al. (2010), for zoisite eclogites and the zoisite vein by Halama et al. (2010).

Fig. 14. Primitive mantle-normalized (McDonough and Sun, 1995) trace-element contents for deserpentinized chlorite harzburgite (SEC41-2, see Table 4, electronic supplement) compared to antigorite peridotites (John et al., 2010).

Table Titles

Table 1

Selected LA-ICP-MS analyses of trace elements in zoisite, omphacite and fluid inclusion-rich omphacite domains.

Table 2

Major-element (XRF) and trace-element (ICP-MS) analysis of chlorite harzburgite.

Research Highlights

High-P zoisite veins and metasomatized eclogites indicate fluid flow at 70 km depth.
External homogeneous low-salinity H_2O-NaCl-CH_4-CO_2 fluid infiltrates eclogites.
Trace elements (REE, Pb, Sr, Th, U) are transported in high-pressure zoisite veins.
Deserpentinized spinifex-textured chlorite harzburgite is the potential fluid source.
Dehydration fluid leached metabasites and metapelites by fluid-rock interaction.

.

Table 1

Mineral	Omphacite									Zoisite						
Sample	SEC13-4	SEC13-4	SEC31-2-:	SEC27-2	SEC27-2	SEC27-2	SEC29-2	SEC29-2	SEC29-2	SEC27-1	SEC27-2	SEC27-2	SEC29-2	SEC31-2-1	SEC31-2-1	SEC31-2-2
Analysis	3	5	2	8	9	10	1	3	2	12	4	5	17	20	21	10
Comment				Core	Core with fluid incl.	Rim	Core	Core with fluid incl.	Rim							
Rock type	MTEC	MTEC	ZEC	ZEC	ZEC	ZEC	ZEC	ZEC	ZEC	ZEC	ZV	ZV	ZV	ZV	ZV	ZEC
Li	186	235	217	175	184	156	202	180	205	0.4	0.3	0.2	0.9	<0.2	1.8	0.4
Be	0.8	1.3	3.4	3.4	3.3	2.7	3.1	4.5	3.4	0.2	0.2	<0.1	<0.1	<0.1	<0.1	<0.1
B	4.6	2.2	2.1	1.3	5.4	1.9	2.2	5.7	1.8	0.5	<0.4	<0.8	<0.4	0.9	1.2	1.0
Sc	65	59	13	20	24	14	17	34	18	13	14	4	18	7	17	10
Ti	1770	930	600	540	620	504	446	560	520	620	730	332	620	620	670	990
Cr	221	415	385	307	338	176	113	90	129	430	248	70	135	25	192	327
Ni	47	82	56	60	74	51	58	86	110	0.4	0.5	0.5	1.1	0.3	0.4	0.6
Rb	<0.04	<0.04	<0.04	<0.04	0.06	<0.04	<0.04	0.09	<0.04	<0.02	<0.02	<0.02	<0.02	<0.02	<0.02	<0.02
Sr	123	65	15	25	24	21	21	44	20	3540	7190	8230	4530	5600	6030	2720
Y	2.0	1.5	0.15	0.12	0.20	0.11	0.11	0.38	0.25	11	47	19	38	11	79	13
Zr	12	4	1.7	1.5	1.7	1.3	0.9	1.7	1.2	2.1	4	0.5	3.4	3.4	3.3	7
Nb	<0.04	<0.04	0.08	0.15	0.08	0.07	<0.04	0.06	0.04	<0.03	<0.03	<0.03	<0.03	<0.03	<0.03	<0.03
Cs	<0.02	<0.02	<0.02	<0.02	<0.02	<0.02	<0.02	<0.02	<0.02	<0.02	<0.02	<0.02	<0.02	0.03	0.04	<0.02
Ba	<0.02	<0.02	<0.02	0.52	0.86	0.26	0.23	0.68	0.42	5	5.6	9.8	6.0	8.0	8.7	8.3
La	<0.03	<0.03	<0.03	<0.03	<0.03	<0.03	<0.03	<0.03	<0.03	38	180	83	503	27	623	62
Ce	0.29	0.07	<0.02	<0.02	<0.02	<0.02	<0.02	0.03	<0.02	75	370	172	1280	52	1407	119
Pr	0.12	<0.02	<0.02	<0.02	<0.02	<0.02	<0.02	<0.02	<0.02	10	49	21	132	7	157	16
Nd	1.5	<0.2	<0.2	<0.2	<0.2	<0.2	<0.2	<0.2	<0.2	44	196	82	516	30	624	61
Sm	1.0	0.26	<0.15	<0.15	<0.15	<0.15	<0.15	<0.15	<0.15	13	40	17	111	7	128	12
Eu	0.77	0.29	<0.04	<0.04	<0.04	<0.04	<0.04	<0.04	<0.04	3	9	5	22	2	28	3
Gd	2.8	1.1	<0.2	<0.2	<0.2	<0.2	<0.2	<0.2	<0.2	10	33	15	76	7	95	9
Tb	0.33	0.12	<0.02	<0.02	<0.02	<0.02	<0.02	0.02	<0.02	1.1	3.5	1.5	6.4	1.0	9	0.9
Dy	0.64	0.53	<0.1	<0.1	0.12	<0.1	<0.1	<0.1	0.18	3.5	13.7	5.9	19	3.1	33	3.9
Ho	0.05	<0.03	<0.03	<0.03	<0.03	<0.03	<0.03	<0.03	<0.03	0.4	1.4	0.6	1.7	0.3	3.5	0.5
Er	<0.1	<0.1	<0.1	<0.1	<0.1	<0.1	<0.1	<0.1	<0.1	0.8	2.7	1.3	2.7	0.6	6.5	1.0
Tm	<0.03	<0.03	<0.03	<0.03	<0.03	<0.03	<0.03	<0.03	<0.03	0.12	0.25	0.10	0.21	0.04	0.41	0.10
Yb	<0.1	<0.1	<0.1	<0.1	<0.1	<0.1	<0.1	<0.1	<0.1	0.55	1.06	0.26	0.59	0.28	1.84	0.54
Lu	<0.03	<0.03	<0.03	<0.03	<0.03	<0.03	<0.03	<0.03	<0.03	0.10	0.08	0.02	0.09	<0.02	0.11	0.06
Hf	0.98	0.27	0.19	<0.1	0.15	0.15	0.16	<0.1	0.16	0.17	0.16	0.06	0.24	0.14	0.19	0.39
Ta	<0.04	<0.04	<0.04	<0.04	<0.04	<0.04	<0.04	<0.04	<0.04	<0.02	<0.02	<0.02	<0.02	<0.02	<0.02	<0.02
Pb	4.1	1.2	1.0	3.4	92	1.3	0.52	3.3	0.55	61	87	170	94	85	153	66
Th	<0.05	<0.05	<0.05	<0.05	0.05	<0.05	<0.05	<0.05	<0.05	1.5	90	18	190	4	215	12
U	<0.04	<0.04	<0.04	<0.04	<0.04	<0.04	<0.04	<0.04	<0.04	4.4	21	7	36	3.8	49	4.5

MTEC = MORB-type eclogite, ZEC = zoisite eclogite, ZV = zoisite vein; concentrations in μg/g.

Table 2

Rock-type	Chlorite harzburgite
Sample	SEC 41-2
Major elements (mass %)	
SiO_2	43.21
TiO_2	0.04
Al_2O_3	3.79
Fe_2O_3	8.06
MnO	0.12
MgO	34.16
CaO	0.67
Na_2O	0.00
K_2O	0.01
P_2O_5	0.01
LOI	9.92
Total	99.99
Trace elements (□g/g)	
Cs	0.374
Rb	0.497
Ba	3.105
Th	0.014
U	0.003
Nb	0.044
Ta	0.019
La	0.050
Ce	0.109
Pb	0.156
Pr	0.016
Sr	4.163
Nd	0.082
Sm	0.027
Zr	0.000
Hf	0.007
Eu	0.011
Ti	0.008
Gd	0.038
Tb	0.007
Dy	0.055
Li	0.839
Ho	0.014
Y	0.372
Er	0.045
Tm	0.008
Yb	0.069
Lu	0.013

al. (2011) and Garbe-Schönberg (1993)

Figure 1

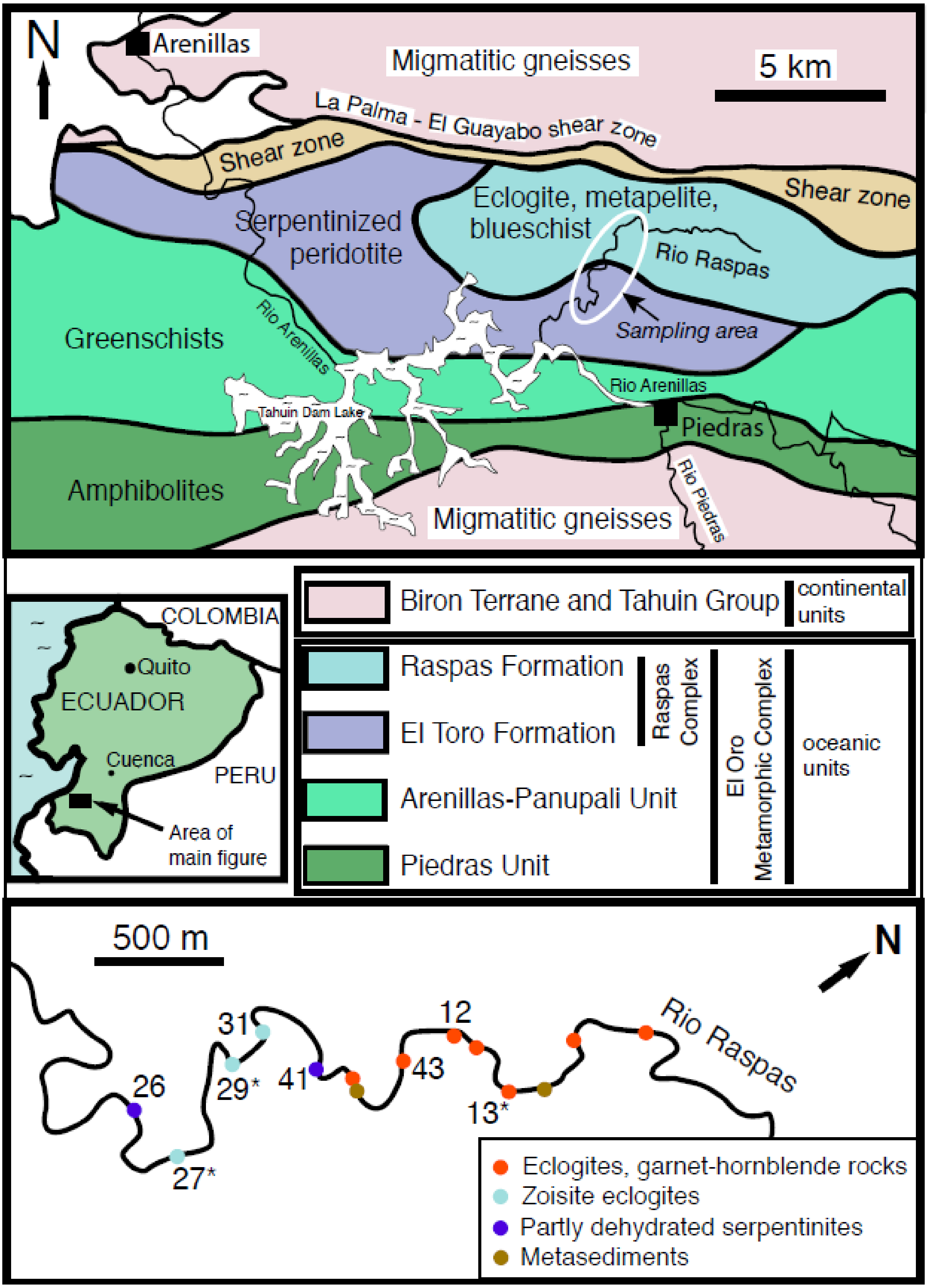
N
Arenillas
Migmatitic gneisses
5 km
La Palma - El Guayabo shear zone
Shear zone
Shear zone
Serpentinized peridotite
Eclogite, metapelite, blueschist
Rio Raspas
Sampling area
Greenschists
Rio Arenillas
Rio Arenillas
Tahuin Dam Lake
Piedras
Amphibolites
Rio Piedras
Migmatitic gneisses
COLOMBIA
Quito
ECUADOR
Cuenca
PERU
Area of main figure
Biron Terrane and Tahuin Group
continental units
Raspas Formation
El Toro Formation
Raspas Complex
Arenillas-Panupali Unit
Piedras Unit
El Oro Metamorphic Complex
oceanic units
500 m
N
Rio Raspas
31
29*
41
12
43
13*
26
27*
Eclogites, garnet-hornblende rocks
Zoisite eclogites
Partly dehydrated serpentinites
Metasediments

Figure 2

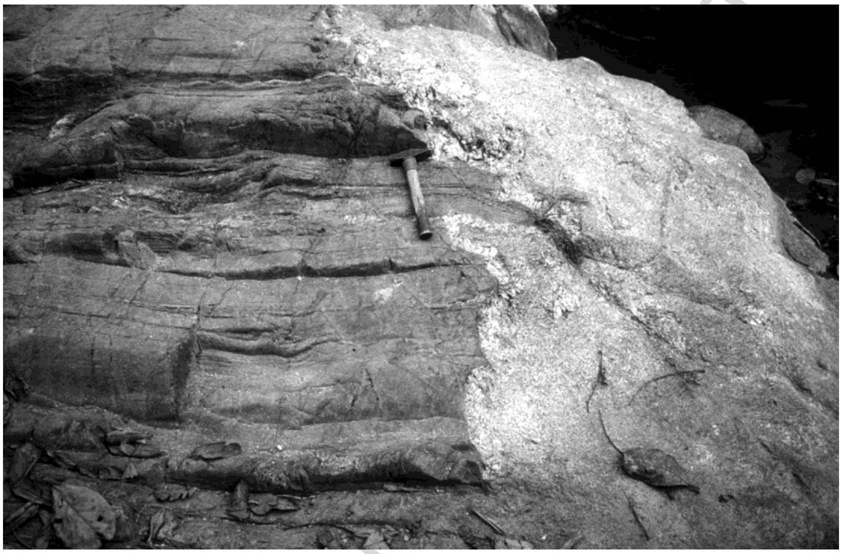

Figure 3

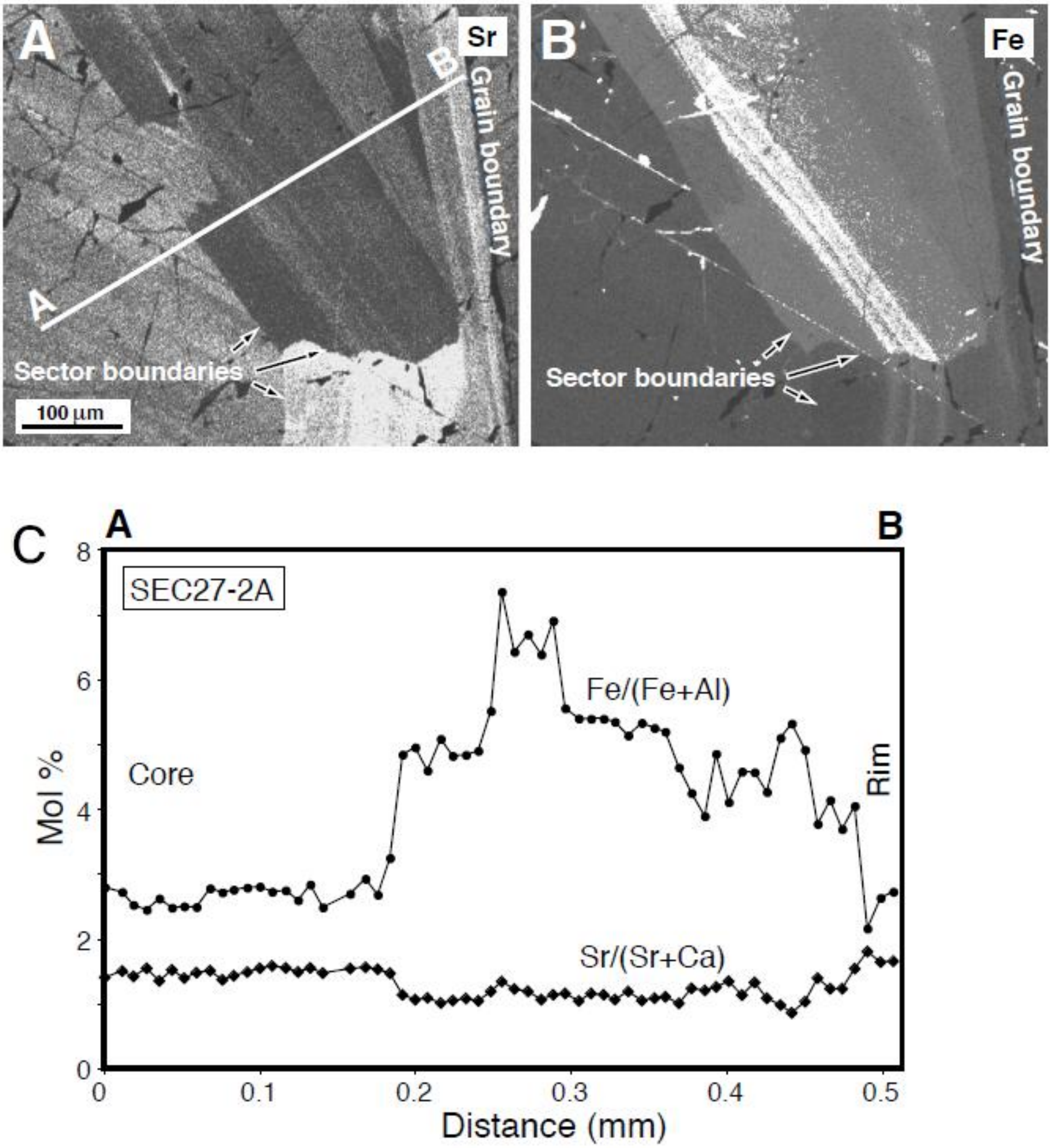
A
Sr
B
A
Grain boundary
Sector boundaries
100 µm
B
Fe
Grain boundary
Sector boundaries
C
A
B
SEC27-2A
Fe/(Fe+Al)
Core
Rim
Sr/(Sr+Ca)
Mol %
Distance (mm)
0
2
4
6
8
0
0.1
0.2
0.3
0.4
0.5

Figure 4 color

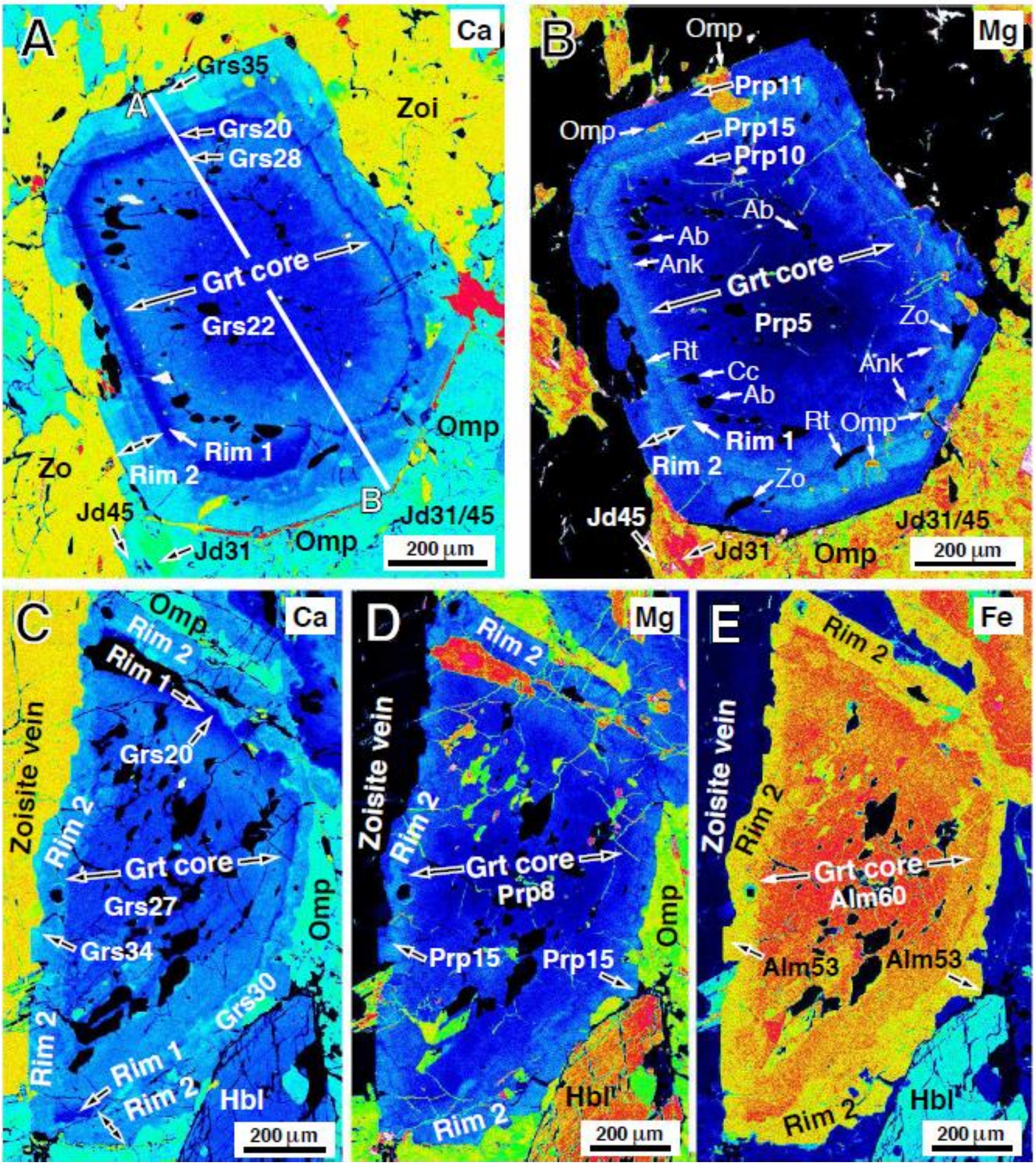

Figure 5

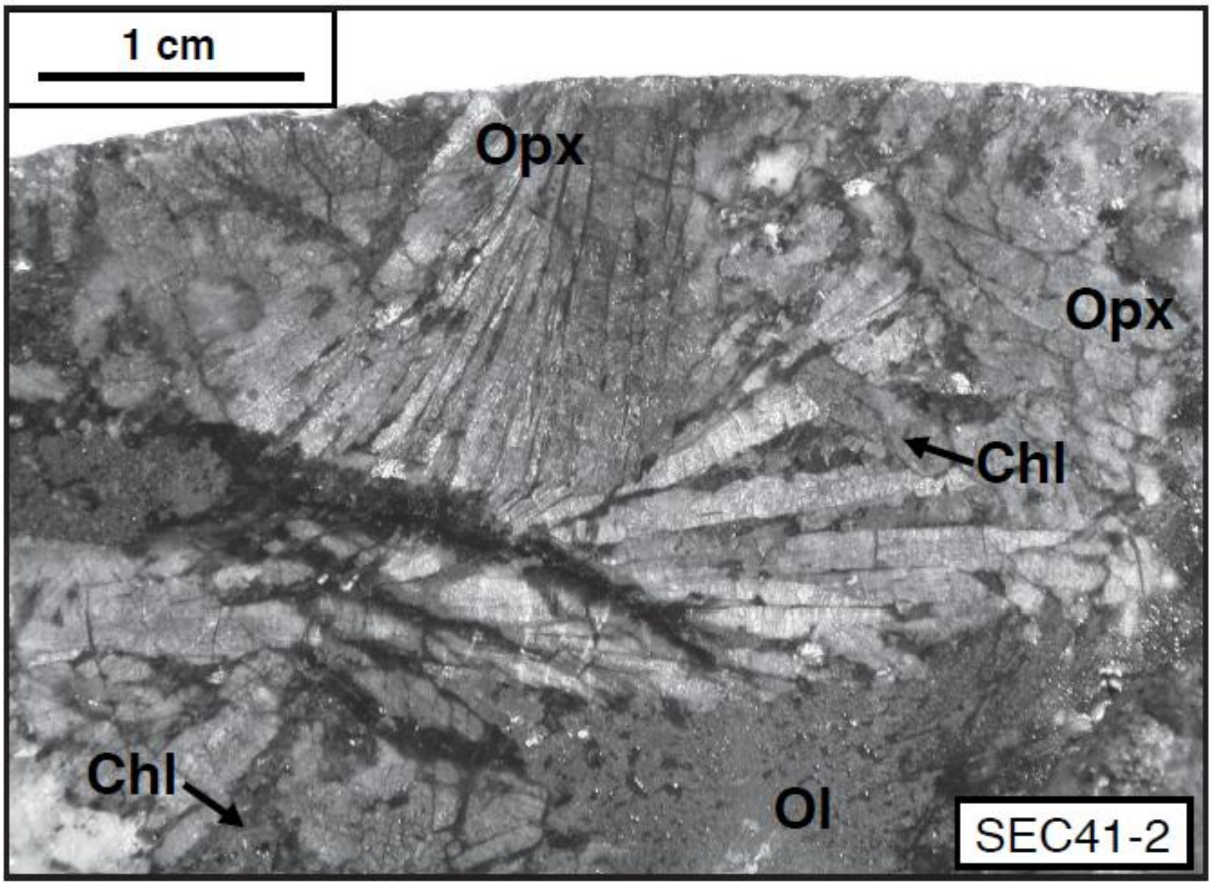

Figure 6

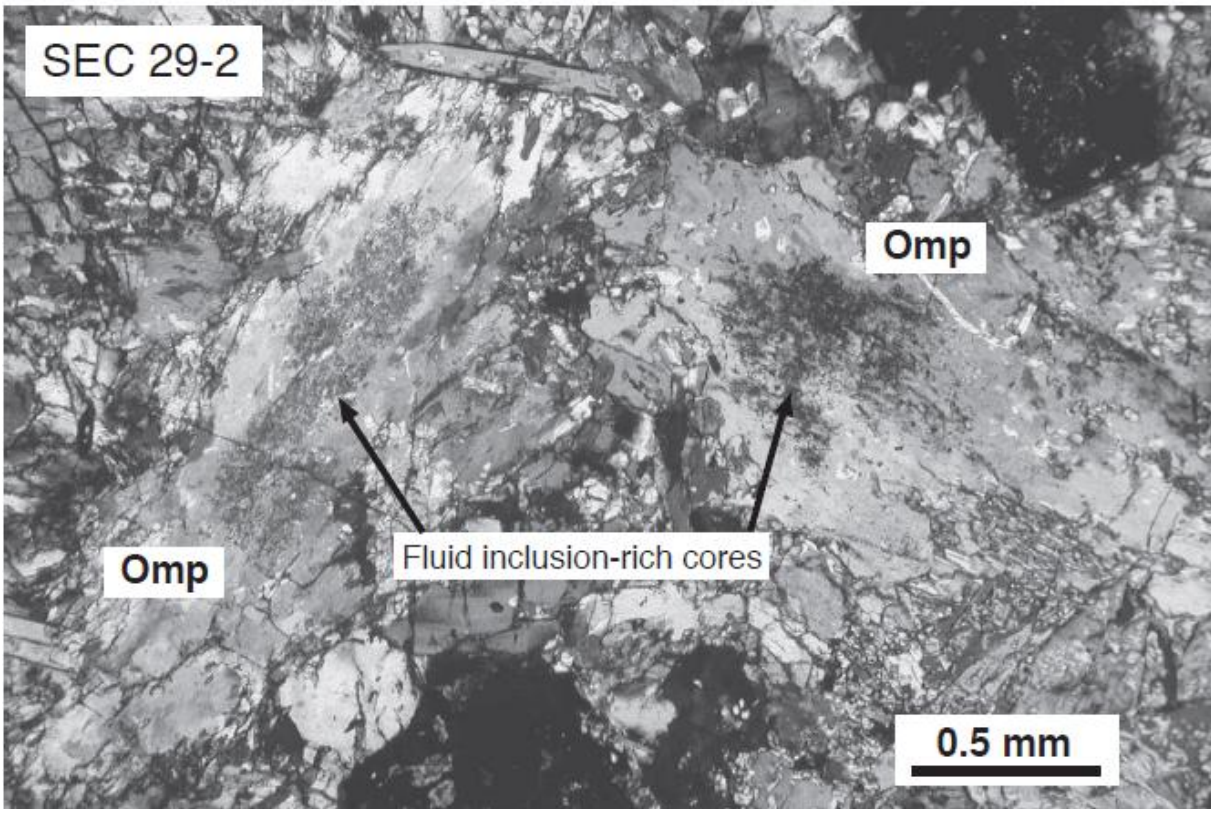

Figure 7

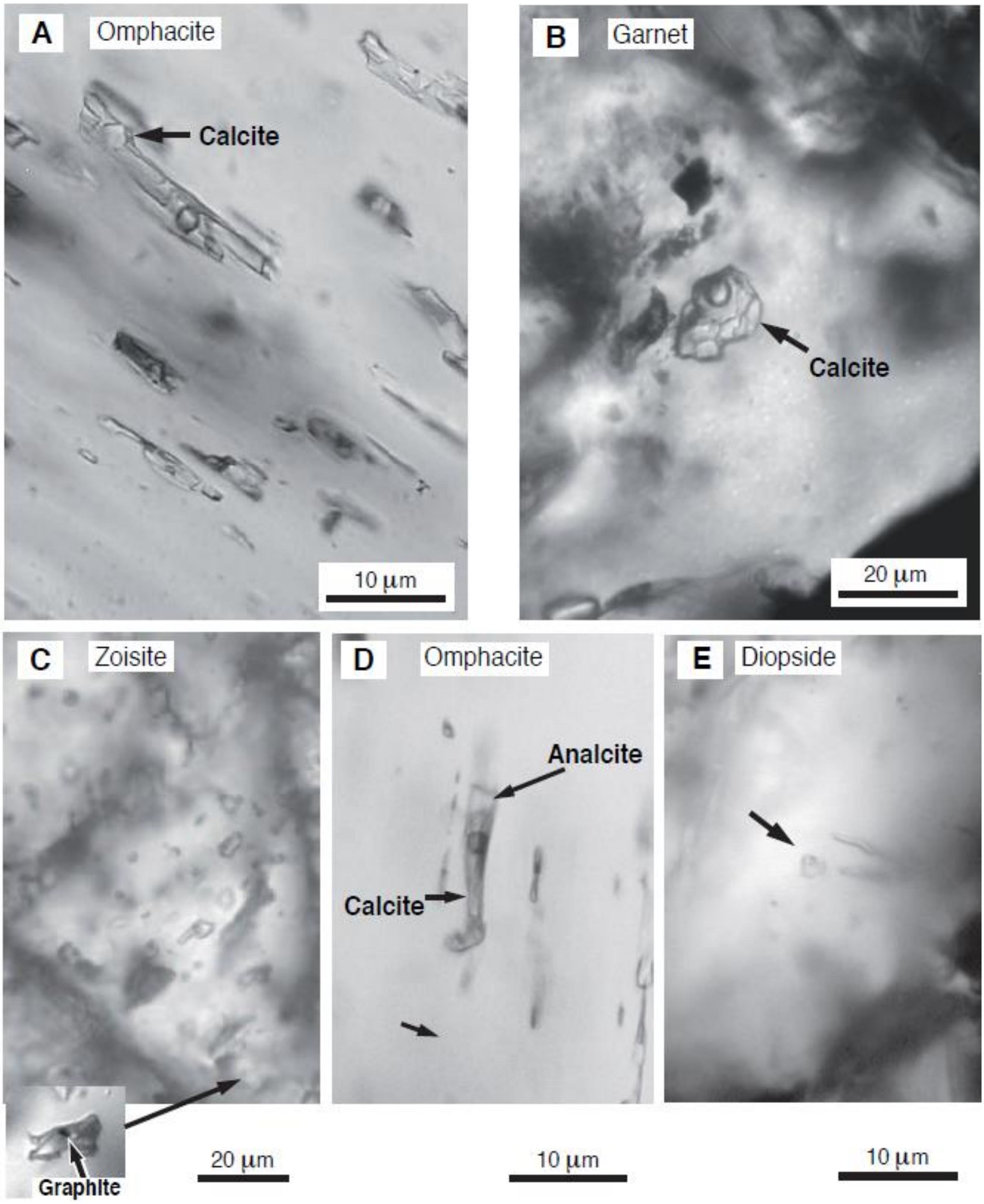
A
Omphacite
Calcite
10 µm
B
Garnet
Calcite
20 µm
C
Zoisite
Graphite
20 µm
D
Omphacite
Analcite
Calcite
10 µm
E
Diopside
10 µm

Figure 8

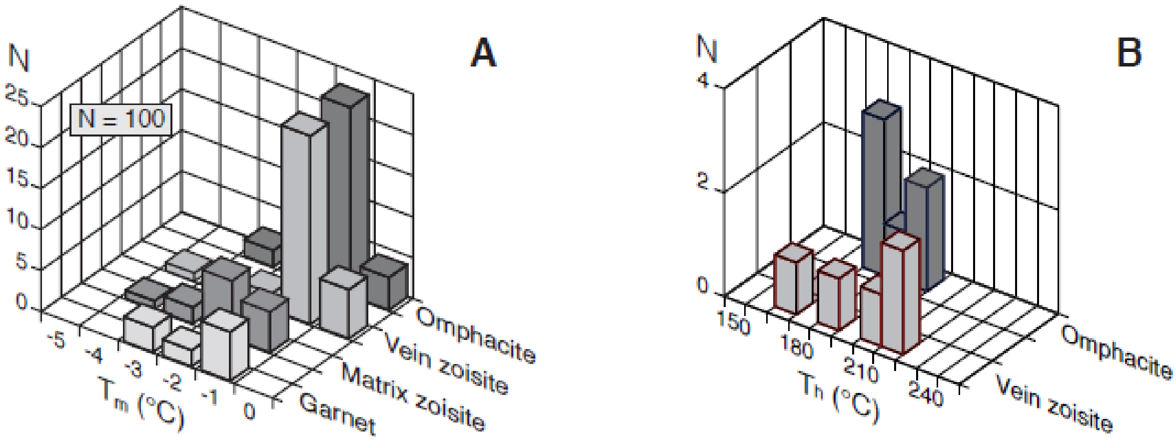
A
N
25
20
15
10
5
0
N = 100
-5
-4
-3
-2
-1
0
T_m (°C)
Omphacite
Vein zoisite
Matrix zoisite
Garnet
B
N
4
2
0
150
180
210
240
T_h (°C)
Omphacite
Vein zoisite

Figure 9

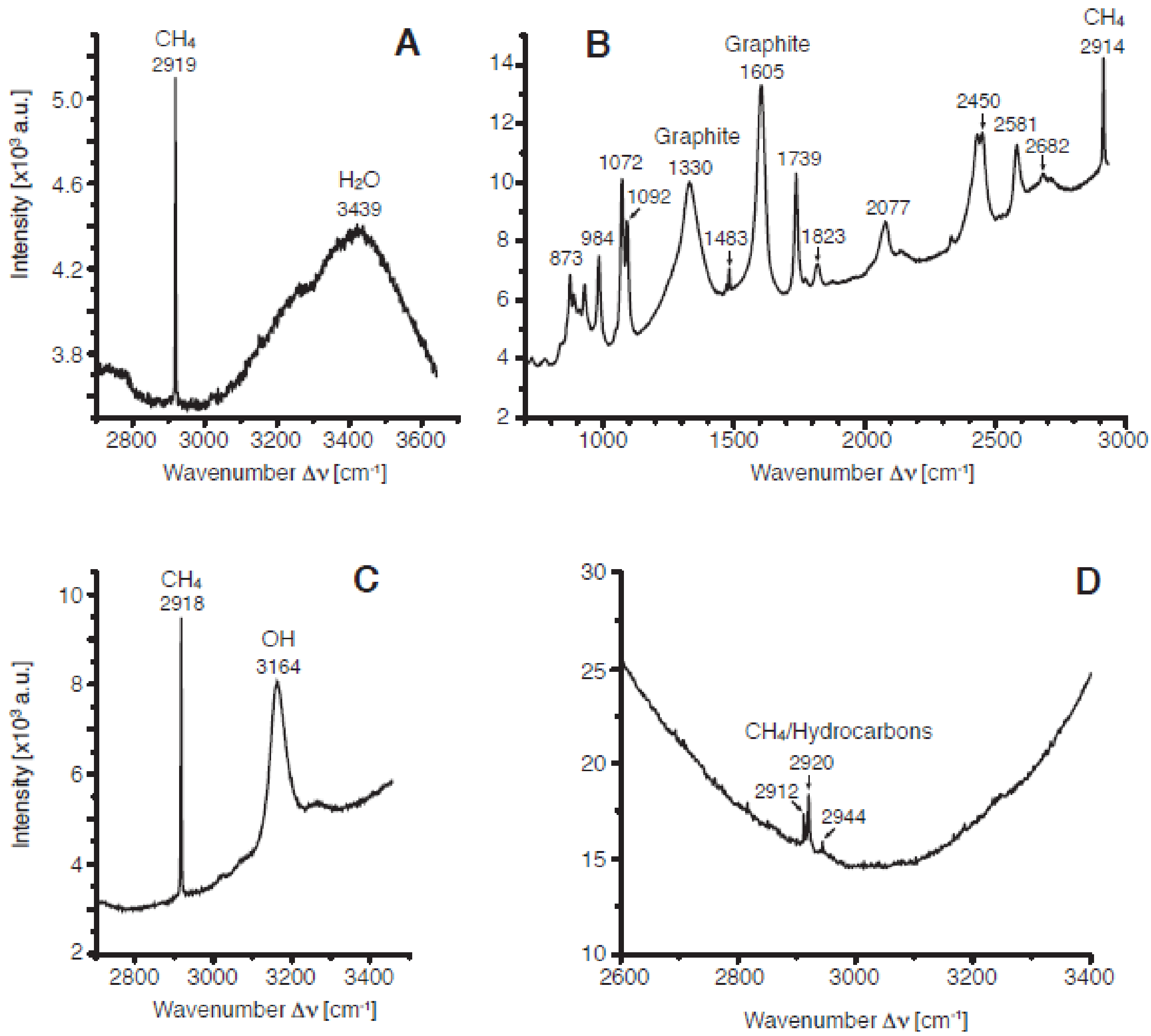
A
CH4
2919
H2O
3439
Intensity [x10³ a.u.]
Wavenumber Δν [cm⁻¹]
B
Graphite
1605
Graphite
1330
CH4
2914
873
984
1072
1092
1483
1739
1823
2077
2450
2581
2682
C
CH4
2918
OH
3164
D
CH4/Hydrocarbons
2920
2912
2944

Figure 10

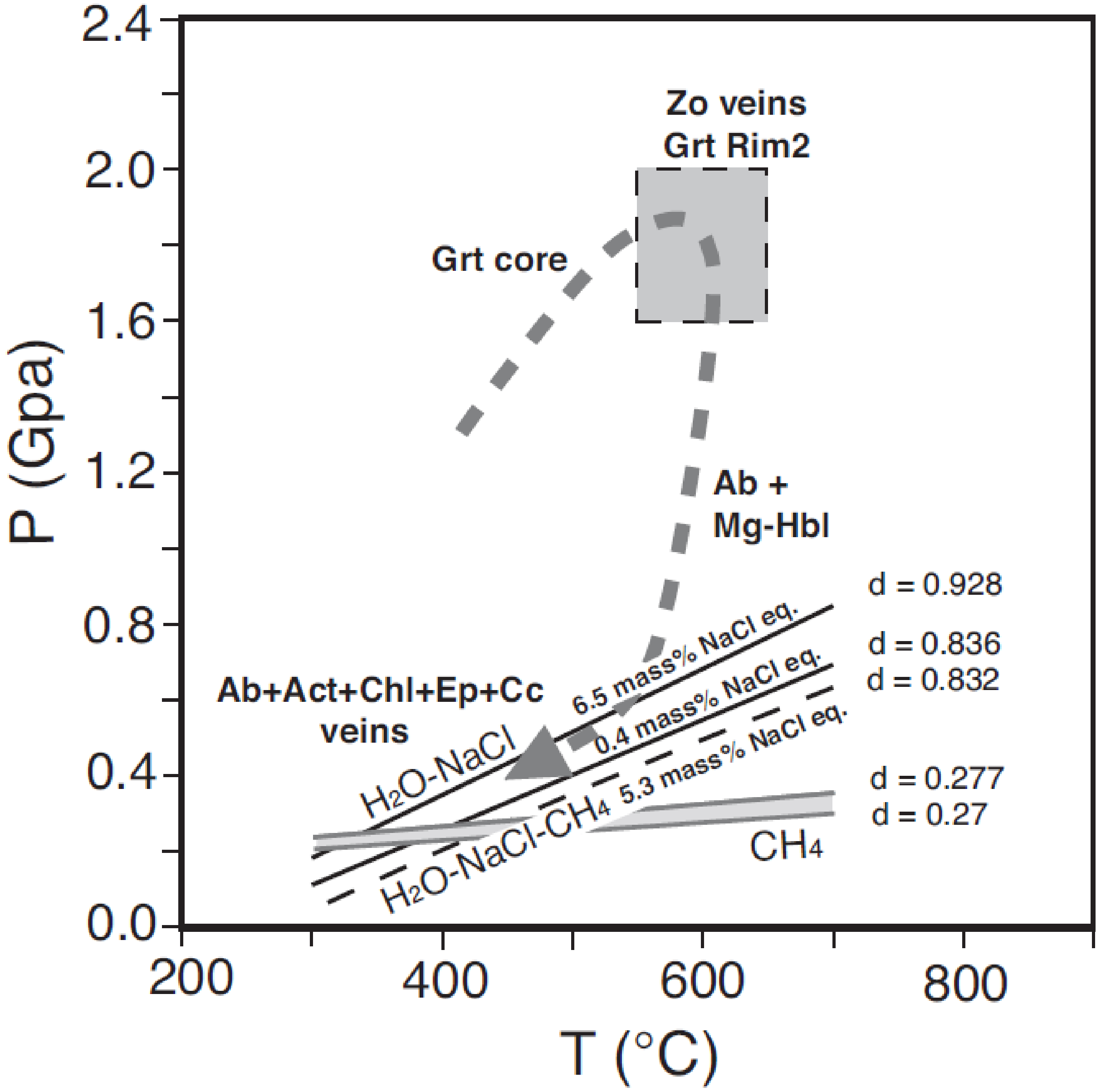

2.4
2.0
1.6
1.2
0.8
0.4
0.0
P (Gpa)
200
400
600
800
T (°C)
Zo veins
Grt Rim2
Grt core
Ab +
Mg-Hbl
Ab+Act+Chl+Ep+Cc
veins
H2O-NaCl
H2O-NaCl-CH4
6.5 mass% NaCl eq.
0.4 mass% NaCl eq.
5.3 mass% NaCl eq.
d = 0.928
d = 0.836
d = 0.832
d = 0.277
d = 0.27
CH4

Figure 11

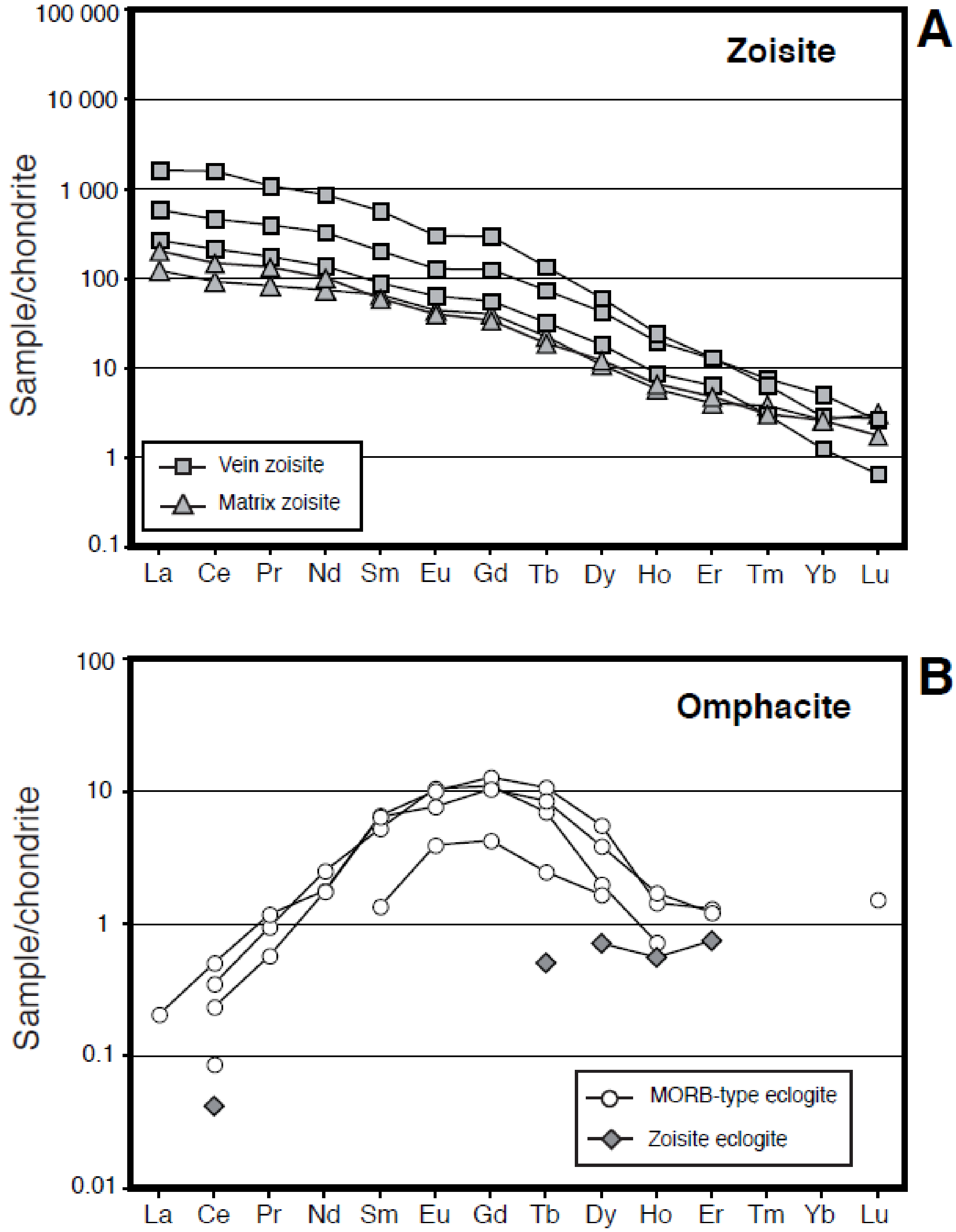
Zoisite
A
Sample/chondrite
100 000
10 000
1 000
100
10
1
0.1
Vein zoisite
Matrix zoisite
La
Ce
Pr
Nd
Sm
Eu
Gd
Tb
Dy
Ho
Er
Tm
Yb
Lu
Omphacite
B
100
10
1
0.1
0.01
MORB-type eclogite
Zoisite eclogite

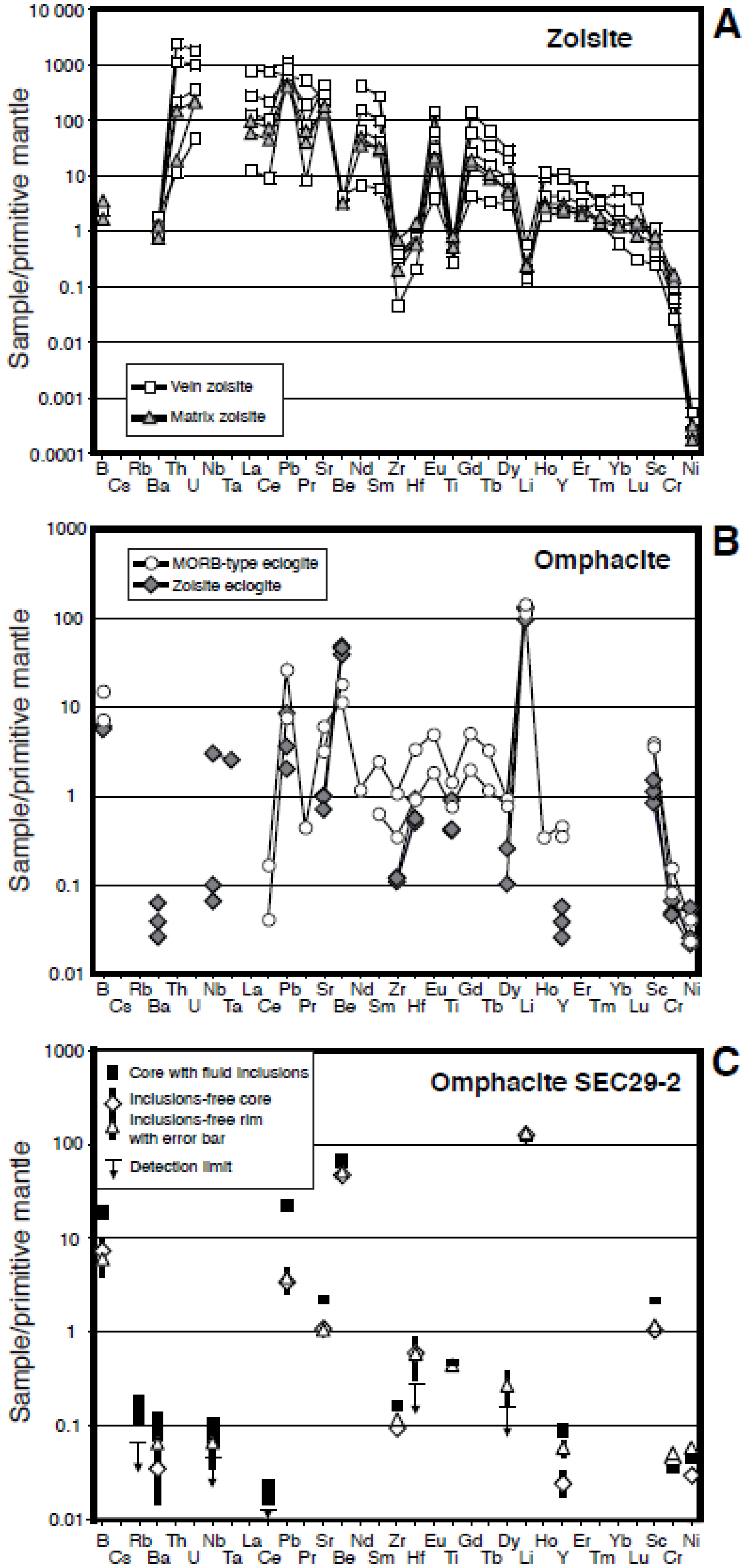
A
Zoisite
Vein zoisite
Matrix zoisite
Sample/primitive mantle
10 000
1000
100
10
1
0.1
0.01
0.001
0.0001
B Rb Th Nb La Pb Sr Nd Zr Eu Gd Dy Ho Er Yb Sc Ni
Cs Ba U Ta Ce Pr Be Sm Hf Ti Tb Li Y Tm Lu Cr
B
Omphacite
MORB-type eclogite
Zoisite eclogite
Sample/primitive mantle
1000
100
10
1
0.1
0.01
B Rb Th Nb La Pb Sr Nd Zr Eu Gd Dy Ho Er Yb Sc Ni
Cs Ba U Ta Ce Pr Be Sm Hf Ti Tb Li Y Tm Lu Cr
C
Omphacite SEC29-2
Core with fluid inclusions
Inclusions-free core
Inclusions-free rim
with error bar
Detection limit
Sample/primitive mantle
1000
100
10
1
0.1
0.01
B Rb Th Nb La Pb Sr Nd Zr Eu Gd Dy Ho Er Yb Sc Ni
Cs Ba U Ta Ce Pr Be Sm Hf Ti Tb Li Y Tm Lu Cr

Figure 12

Figure 13

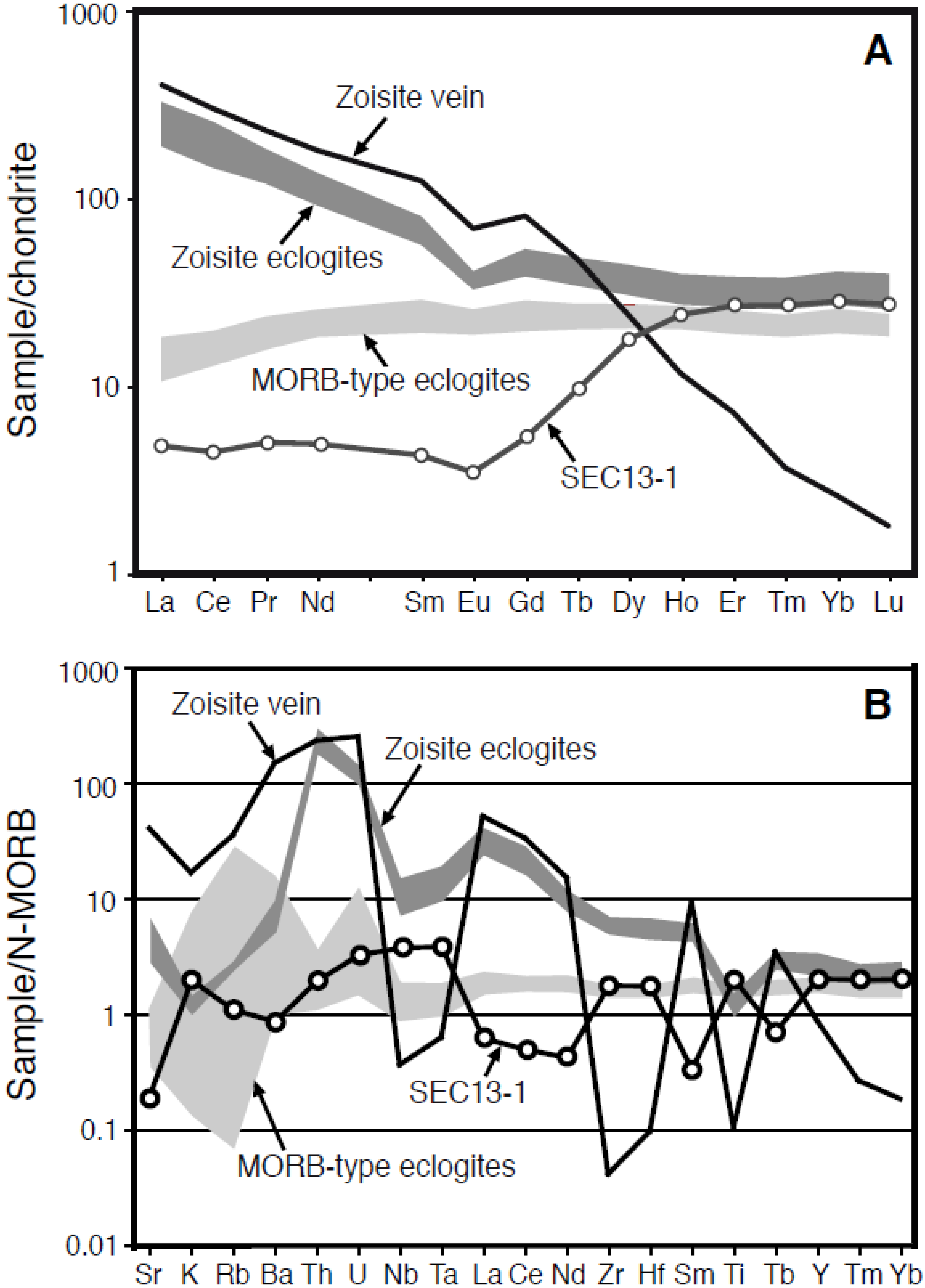
1000
100
10
1
Sample/chondrite
A
Zoisite vein
Zoisite eclogites
MORB-type eclogites
SEC13-1
La Ce Pr Nd Sm Eu Gd Tb Dy Ho Er Tm Yb Lu
1000
100
10
1
0.1
0.01
Sample/N-MORB
B
Zoisite vein
Zoisite eclogites
SEC13-1
MORB-type eclogites
Sr K Rb Ba Th U Nb Ta La Ce Nd Zr Hf Sm Ti Tb Y Tm Yb

Figure 14

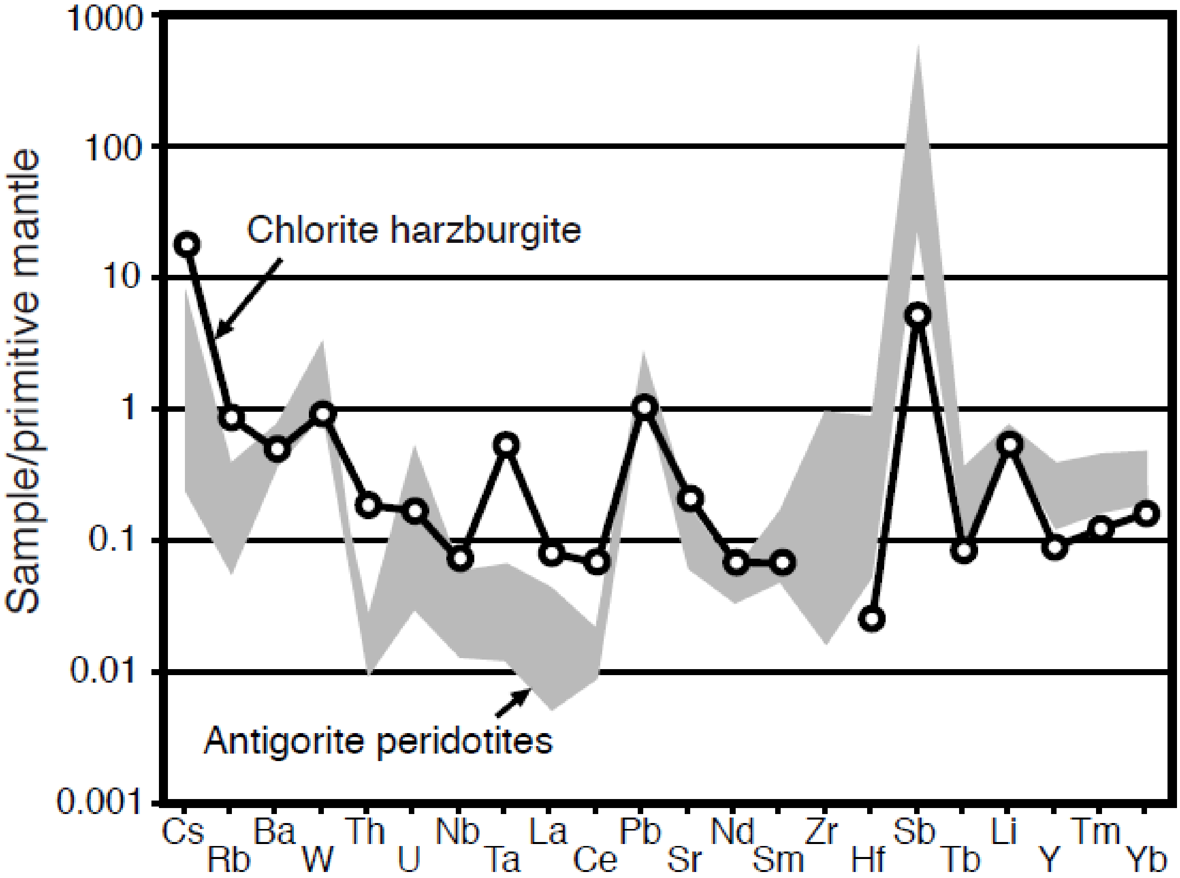
1000
100
10
1
0.1
0.01
0.001
Sample/primitive mantle
Chlorite harzburgite
Antigorite peridotites
Cs
Rb
Ba
W
Th
U
Nb
Ta
La
Ce
Pb
Sr
Nd
Sm
Zr
Hf
Sb
Tb
Li
Y
Tm
Yb